ACS OMEGA

http://pubs.acs.org/journal/acsodf

Article

Cyclodextrin-Assisted Surface-Enhanced Photochromic Phenomena of Tungsten(VI) Oxide Nanoparticles for Label-Free Colorimetric Detection of Phenylalanine

Kenta Adachi,* Hiro Azakami, Miyuki Yamauchi, Moeka Koshoji, Asami Yamamoto, and Shohei Tanaka

Cite This: *ACS Omega* 2024, 9, 18957−18972

Read Online

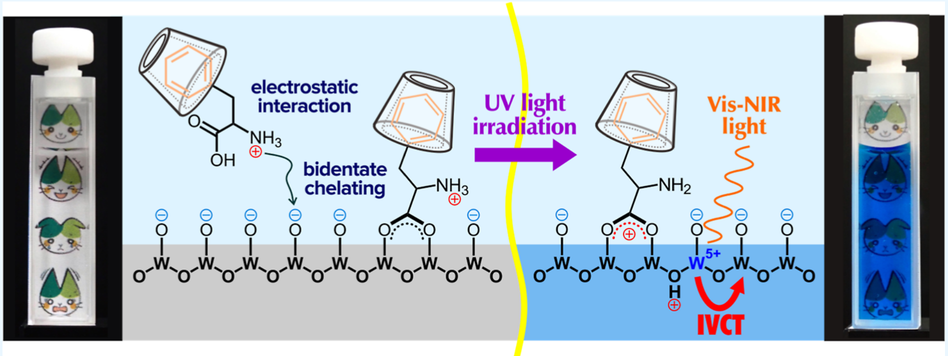

ABSTRACT: Herein are presented the results of experiments designed to evaluate the effectiveness of host−guest interactions in improving the sensitivity of colorimetric detection based on surface-enhanced photochromic phenomena of tungsten(VI) oxide (WO_3) nanocolloid particles. The UV-induced photochromic coloration of WO_3 nanocolloid particles in the presence of aromatic α-amino acid (AA), L-phenylalanine (Phe) or L-2-phenylglycine (Phg), and heptakis(2,3,6-tri-*O*-methyl)-β-cyclodextrin (TMβCDx) in an aqueous system was investigated using UV−vis absorption spectrometry. The characteristics of the adsorption modes and configurations of AAs on the WO_3 surface have also been identified by using a combination of adsorption isotherm analysis and attenuated total reflection Fourier transform infrared spectroscopy (ATR-FTIR). A distinct linear relationship was observed between the concentration of AAs adsorbed on the WO_3 nanocolloid particles and the initial photochromic coloration rate in the corresponding UV-irradiated colloidal WO_3 in aqueous media, indicating that a simple and sensitive quantification of AAs can be achieved from UV-induced WO_3 photochromic coloration without any complicated preprocessing. The proposed colorimetric assay in the Phe/TMβCDx/WO_3 ternary aqueous system had a linear range of 1×10^{-8} to 1×10^{-4} mol dm^{-3} for Phe detection, with a limit of detection of 8.3×10^{-9} mol dm^{-3}. The combined results from UV−vis absorption, ATR-FTIR, and adsorption isotherm experiments conclusively indicated that the TMβCDx-complexed Phe molecules in the Phe/TMβCDx/WO_3 ternary aqueous system are preferentially and strongly inner-sphere adsorbed on the WO_3 surface, resulting in a more significant surface-enhanced photochromic phenomenon. The findings in this study provided intriguing insights into the design and development of the “label-free” colorimetric assay system based on the surface-enhanced photochromic phenomenon of the WO_3 nanocolloid probe.

1. INTRODUCTION

Amino acids play important roles in various essential metabolic processes, and their homeostasis is necessary for cell survival and healing.[1,2] For instance, fluctuations in the concentration of L-phenylalanine (Phe), a proteinaceous L-α-amino acid compound in humans, cause metabolic abnormalities.[3] Phenylketonuria is a disease in which phenylalanine accumulates in the body. The excessive buildup of Phe will lead to brain damage and mental retardation.[4,5] Accordingly, a simple, rapid, and highly sensitive monitoring system for detecting Phe is vital for disease diagnosis. Several detection approaches have been developed to quantify amino acids in biological fluids, including aptasensor, chemiluminescence, enzymatic colorimetric sensor, electrochemical sensor, Laser-induced fluorescence, surface plasmon resonance (SPR) sensor, and whole-cell biosensor.[6−16] However, most of these methods require expensive equipment and skilled operation experience, making amino acid quantification assays and protocols more complicated. The comparative studies [method, linearity

Received: November 20, 2023
Revised: February 13, 2024
Accepted: February 20, 2024
Published: April 15, 2024

https://doi.org/10.1021/acsomega.3c09239
ACS Omega 2024, 9, 18957−18972

Table 1. Comparison of Various Detection Methods in the Literatures for Determination of Phe[a]

detection method	linear range/mol dm^{-3}	LOD/mol dm^{-3}	ref
carbon nanosphere electrode	1.0×10^{-6}–1.0×10^{-4}	1.0×10^{-6}	6
chemiluminescence	1.5×10^{-8}–1.2×10^{-7}	2.4×10^{-10}	7
DNA-aptasensor	7.2×10^{-7}–6.0×10^{-3}	2.3×10^{-7}	8
electrochemical biosensor	5.0×10^{-7}–1.5×10^{-2}	4.2×10^{-7}	9
electrochemical sensor	5.0×10^{-7}–1.0×10^{-4}	1.0×10^{-8}	10
enzymatic colorimetric sensor	1.0×10^{-5}–3.0×10^{-3}	1.9×10^{-5}	11
laser-induced fluorescence	1.0×10^{-5}–1.5×10^{-3}	3.0×10^{-6}–5.0×10^{-5}	12,13
optical biosensor	1.0×10^{-5}–1.0×10^{-2}	5.0×10^{-6}	14
SPR sensor	5.0×10^{-6}–4.0×10^{-4}	1.7×10^{-7}	15
whole-cell biosensor	5.0×10^{-6}–5.0×10^{-5}	4.8×10^{-6}	16

[a]LOD: limit of detection.

range, and limit of detection (LOD)] on the determination of Phe in the literature are given in Table 1. Strategic development of phenylalanine colorimetric sensing that can demonstrate new selectivity patterns is of fundamental importance in disease diagnosis, treatment, and prevention, since the use of assays based on new mechanisms is often necessary to achieve the breakthrough. Naked-eye colorimetric detection has attracted widespread attention from the viewpoint of point-of-care testing due to its highly sensitive visible readout, low cost, and no requirement for advanced types of equipment.[17,18] In particular, colorimetric detection using nanoparticles, benefiting from recent advances in nanotechnology, has been developed as a promising technique for healthcare applications.[19]

Some transition metal oxides show an interesting photochromic effect and can be deeply colored by exposing the material to irradiation with appropriate energy.[20,21] Such photochromic phenomena of transition metal oxides have attracted considerable attention because they can be applied to display devices, erasable optical memory media, chemical sensors, smart-windows, and other cutting-edge applications.[22,23] Among them, tungsten(VI) oxide (WO_3), a wide-bandgap *n*-type semiconductor, is mainly the most studied among inorganic photochromic materials because it has characteristics such as chemical stability, coloring efficiency, and fast coloring response time.[24] Many researchers have reported that the hybridization between WO_3 nanomaterials and organic constituents enhances photochromic performance and consider that the monolayer of organic molecules surrounding WO_3 nanomaterials can behave as an active form of organized organic matter.[25−27] This unique enhanced photochromic phenomenon by organic molecules adsorbed on the metal oxide surface is called "surface-enhanced photochromic phenomenon".[28] Recently, we have focused on the surface-enhanced photochromic phenomena of colloidal WO_3 in aqueous media in the presence of amino acid compounds and experimentally demonstrated the usefulness of WO_3 nanoparticles as a colorimetric probe for high-sensitive "label-free" detection of amino acid compounds.[29]

Cyclodextrins (CDxs) are cyclic oligosaccharides consisting of 6, 7, or 8 α-D-glucopyranose units linked by $\alpha(1 \rightarrow 4)$ bonds, usually called α-, β-, and γ-cyclodextrins, respectively. CDx molecule has a truncated cone shape like a bottomless bucket with an inner hydrophobic and an outer hydrophilic surface. Due to their internal spatial structure, CDx and their derivatives can easily form inclusion complexes with guest molecules.[30] Confinement in the hydrophobic cavity can dramatically alter the physicochemical properties of the guest molecule, such as solubility, chemical stability, antioxidant activity, and bioavailability.[31,32] For this reason, CDx and their derivatives are not only used for basic research in various fields such as analytical chemistry, synthetic chemistry, and supramolecular science but also for application development in pharmaceutical technologies such as artificial enzyme reactions, molecular recognition, chiral separation, photodynamic therapy, and drug delivery.[33−36] Despite such extensive research, the adsorption phenomenon of CDx-complexed amino acid molecules on solid surfaces, aiming at developing a novel colorimetric sensing platform for amino acid ones, has yet to receive much attention.

Herein, we report the effect of adding cyclodextrin derivative on applying a high-sensitivity label-free amino acid detection assay based on the surface-enhanced photochromic phenomenon of WO_3 nanocolloid particles. The updated assay approach aimed to improve detection sensitivity through three main steps: (a) formation of inclusion complexes between cyclodextrin derivative, heptakis(2,3,6-tri-*O*-methyl)-β-cyclodextrin (TMβCDx), and aromatic amino acid (AA), L-phenylalanine (Phe) or L-2-phenylglycine (Phg), in the aqueous system; (b) competitive adsorption of TMβCDx-complexed AA and free AA molecules to WO_3 nanocolloid particles in the aqueous system; (c) UV light irradiation to the ternary aqueous system in the presence of AA, TMβCDx, and WO_3 nanocolloid particles. The outstanding enhanced photochromic coloration in the AA/TMβCDx/WO_3 ternary aqueous system was the final result, indicating that TMβCDx molecules act as a promoter of the surface-enhanced photochromic phenomenon of WO_3 nanocolloid particles. Our results described here suggest a new direction for simple, sensitive, and universal label-free colorimetric sensing assay designs based on surface-enhanced photochromic phenomenon of various metal oxide nanomaterials.

2. EXPERIMENTAL SECTION

2.1. Materials. Concentrated hydrochloric acid (conc. HCl, 37 wt %, 12 M), sodium tungstate(VI) dihydrate ($Na_2WO_4{\cdot}2H_2O$), and superdehydrated ethanol (EtOH) are of analytical or organic synthesis grade from Junsei Chemical (Tokyo, Japan). As shown in Scheme 1, two aromatic amino acids (AA), L-phenylalanine (Phe) and L-2-phenylglycine (Phg), were obtained from Tokyo Chemical Industry (Tokyo, Japan), and heptakis(2,3,6-tri-*O*-methyl)-β-cyclodextrin (TMβCDx) was purchased from FUJIFILM Wako Pure Chemical (Osaka, Japan). All other chemicals were of reagent grade from Nacalai Tesque (Kyoto, Japan), Kishida Chemical (Kyoto, Japan), or Sigma-Aldrich Chemical (MO, USA) and

https://doi.org/10.1021/acsomega.3c09239
ACS Omega 2024, 9, 18957−18972

Scheme 1. Chemical Structure of L-phenylalanine (Phe), L-2-Phenylglycine (Phg), and Heptakis(2,3,6-tri-*O*-methyl)-β-cyclodextrin (TMβCDx)[a]

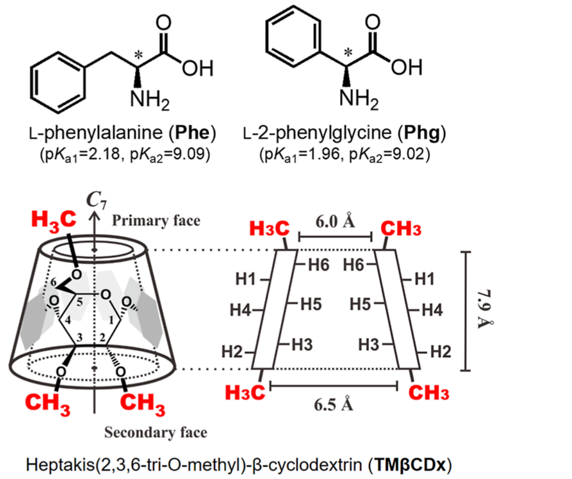

[a]pK_a values of aromatic amino acid compounds from CRC Handbook of Chemistry and Physics (2010).[57]

used as received without further purification. Ultrapure water was prepared using a Milli-Q system (Millipore, USA), resulting in a specific resistivity of 18.2 MΩ cm, and used in all experiments.

2.2. Nanostructured WO_3 Particles. Nanostructured tungsten oxide particles were synthesized via the size-selective dialysis-based sol−gel process using a semipermeable membrane.[37,38] The detailed synthesizing process was as follows. In a typical experiment, $Na_2WO_4{\cdot}2H_2O$ (100 g, 0.3 mol) was dissolved in 100 mL of water under continuous stirring at 25 °C, and afterward adding conc. HCl (7 mL, 0.7 M) dropwisely. A cream white deposit was formed. After efficient stirring for ca. 1 h, a colorless transparent aqueous WO_3 nanocolloid solution (pH 3.3, 0.023 M WO_3) was eventually obtained, which was then closed in a semipermeable tubular membrane (molecular weight cutoff [MWCO] 3500; Cellu-Sep T1, Membrane Filtration Products, Inc., TX, USA) and dialyzed in a 1000 mL beaker containing Milli-Q water for a period of 8 h. The Milli-Q water was periodically replaced until chloride ions could not be detected by ion chromatography. The concentration of chloride ion in the WO_3 colloid solution was determined by using a portable-type IC analyzer (PIA-1000, Shimadzu, Japan) equipped with an anion-exchange Shim-pack IC-A3 column (Shimadzu, Japan) at 30 °C. The eluent used in this study was 4-hydroxybenzoic acid (8.0×10^{-3} M)/bis(2-hydroxyethyl)iminotris(hydroxymethyl)methane (Bis−Tris; 3.2×10^{-3} M), and the flow rate was 300 μL/min. The concentration of the tungsten component in the WO_3 colloid aqueous solution was determined by inductively coupled plasma-atomic emission spectrometry (Liberty Series II, Varian, USA). The as-prepared WO_3 colloid solutions were stable for at least 1 month at room temperature, yielding excellent processability, and refrigerated at 4 °C until used in the experiments. The dried WO_3 colloids were analyzed by X-ray diffraction (RINT-2500, Rigaku, Japan) with CuKα radiation (40 kV, 100 mA) from 2θ = 5 to 75° with a scan speed of 5° min^{-1}. The XRD pattern was indexed to a $WO_3{\cdot}2H_2O$ layered structure in accordance with the JCPDS card no. 18-1420 (see Figure S6 in Supporting Information). The band gap energy of the as-prepared WO_3 nanocolloid particles was determined to be 3.2 eV, corresponding to an indirect band gap of crystalline $WO_3{\cdot}2H_2O$ (see Figure S7 in Supporting Information).[39] The morphology of the as-prepared WO_3 nanocolloid particles was studied by using a transmission electron microscope (JEM-2100, JEOL, Japan). The typical TEM image (Figure S8a in Supporting Information) shows that the as-prepared WO_3 nanocolloid particles is made of a homogeneous phase with particles uniformly sized, which display spherical-like morphology, with a smooth surface. The size distribution histogram of WO_3 nanocolloid particles was assessed by averaging the size of 100 particles directly from TEM images, where the range was from about 8 to 26 nm and the average diameter was estimated as 21.4 nm (see Figure S8a in Supporting Information).

The pH-dependent surface charge characterization using a zeta-potential analyzer (ELSZ-2Plus, Otsuka Electronics, Japan) revealed that the as-prepared WO_3 nanocolloid particles in aqueous media had a point of zero charge (PZC) at a pH of around 0.2 which is consistent with the literature value[40] (see Figure S9 in Supporting Information). The zeta-potential values were calculated based on Smoluchowski equation.

2.3. Adsorption of Aromatic Amino Acids on the WO_3 Nanocolloid Particles in the Absence/Presence of TMβCDx. Adsorption of AA molecules on the WO_3 nanocolloid particles in the absence and presence of TMβCDx was investigated by a batch technique at room temperature (25 ± 2 °C) according to the previously reported sequence.[29] Briefly, AA and TMβCDx were dissolved in water separately as stock solutions. As-prepared WO_3 colloid aqueous solution and the TMβCDx stock aqueous solution were diluted sequentially to a series of concentrations and mixed together evenly. Then, the AA aqueous solution would be added and stirred for 30 min at room temperature. The preliminary studies indicated that the adsorption of AA molecules on the WO_3 nanocolloid particles used in this study achieved complete equilibrium within 30 min. The same concentration sequence in the absence of TMβCDx was also run in the identical condition. The aqueous system was adjusted to the desired pH by adding small volumes of 0.01 or 0.1 M HCl or NaOH. The pH values of the AA/TMβCDx/WO_3 ternary and AA/WO_3 binary aqueous solution were periodically checked with an F-14 pH meter (Horiba, Japan) equipped with a 6366-10D glass electrode (Horiba, Japan). After filtration using a disposable filter unit (Ekikuro Disk 25CR, Shimadzu, Japan), the concentration of AAs was determined by HPLC on a CTO-20A (Shimadzu, Japan) system equipped with a guard column and a COSMOSIL Cholester (250 mm L × 4.6 mm i.d., 5 μm) column (Nacalai Tesque, Inc., Japan) with UV detection (SPD-20A, Shimadzu, Japan: at 258 nm for Phe, and 257 nm for Phg), using water (100%) adjusted to ionic strength (0.1 M) with sodium sulfate as an eluent at 1 mL/min and 25 °C. Optimal conditions for the various amino acids were carefully considered and a calibration curve was built. The accuracy of determination of AAs within the studied concentration range was within 5%. Figure S5 in Supporting Information shows a typical HPLC chromatogram obtained in the Phe/TMβCDx/WO_3 ternary aqueous system. We detected (1) WO_3 nanocolloid particles with AA and/or TMβCDx-complexed AA molecules adsorbed on the surface, (2) free AA molecules, and (3) TMβCDx-complexed AA molecules separately. The amount of AA adsorbed on the WO_3 nanocolloid particles could be determined using the difference between the initial and equilibrium concentrations. In the AA/WO_3 binary

https://doi.org/10.1021/acsomega.3c09239
ACS Omega 2024, 9, 18957−18972

aqueous system, the difference between the initial and equilibrium concentrations ($\Delta[\mathrm{AA}]_{\mathrm{bi}}$/mol dm^{-3}) can be written as

$$\Delta[\mathrm{AA}]_{\mathrm{bi}} = [\mathrm{AA}]_{\mathrm{ad}}\frac{S}{V} \tag{1}$$

where $[\mathrm{AA}]_{\mathrm{ad}}$ is the concentration of AA on the WO_3 colloid surface (mol dm^{-2}). On the other hand, in the AA/TMβCDx/WO_3 ternary aqueous system, the difference between the initial and equilibrium concentrations ($\Delta[\mathrm{AA}]_{\mathrm{ter}}$/mol dm^{-3}) can be described as follows

$$\Delta[\mathrm{AA}]_{\mathrm{ter}} = [\mathrm{AA}]_{\mathrm{ad}}\frac{S}{V} + [\mathrm{TM}\beta\mathrm{CDx{\cdot}AA}] \tag{2}$$

Herein, [TMβCDx·AA] refers to the concentration of TMβCDx-complexed AA in the aqueous solution (mol dm^{-3}).

2.4. Photochromic Coloration of Aromatic Amino Acid/WO_3 Binary and Aromatic Amino Acid/TMβCDx/WO_3 Ternary Aqueous Solution. The AA aqueous solution or mixture of AA and TMβCDx aqueous solutions was added to the aqueous solution containing WO_3 colloids and sodium sulfate for ionic strength adjustment. Then, the AA/WO_3 binary and AA/TMβCDx/WO_3 ternary aqueous solution were individually injected into a single compartment cell (1.0 cm path-length) with two quartz windows. Afterward, these binary and ternary aqueous solutions were bubbled with N_2 gas to eliminate the oxygen, and then the cells were tightly sealed. Black lights (FL4BLB, Panasonic, 4 W × 4, λ_{max} = 365 nm) were used as the excitation UV source. The photochromic colorations in the AA/WO_3 binary and AA/TMβCDx/WO_3 ternary aqueous system were measured by using a UV−vis spectrometer (V-730, Jasco, Japan). Photochromic behaviors in the TMβCDx/WO_3 binary aqueous system were also investigated in a similar manner as described above.

2.5. ATR-FTIR Spectroscopic Analysis of Aromatic Amino Acid Adsorbed onto WO_3 Thin Films. According to the reference procedure,[41] the adsorption modes (outer- and inner-sphere adsorption) of AAs was investigated using attenuated total reflectance Fourier-transform infrared (ATR-FTIR) spectroscopy on cast WO_3 nanoparticles' thin film. The ATR-FTIR spectra were collected on a Nicolet iS10 FTIR spectrometer equipped with an MCT detector (Thermo, USA) and a horizontal ATR accessory (PIKE, USA). A multiple 45° reflection AMTIR (Amorphous Material Transmitting Infrared Radiation, $Ge_{33}As_{12}Se_{55}$) crystal prism was attached to the ATR trough-type cell. A total of 256 scans at 4 cm^{-1} resolution were averaged for each spectrum to reduce noise. To create the WO_3 nanoparticles' thin film on the AMTIR crystal, aqueous WO_3 colloid solution (0.023 M WO_3, 2 mL) was added to the flow cell and dried at RT under vacuum for 1 day. Then, the loosely deposited WO_3 nanoparticles were removed from the cast WO_3 film by rinsing with water. At first, a background spectrum of the cast WO_3 nanocolloid particle film immersed in a background aqueous solution containing buffer and sodium sulfate for ionic strength adjustment was collected, followed by a sample spectrum of the cast film immersed in a sample aqueous solution containing aromatic amino acid and TMβCDx with the same pH and ionic strength over sufficient time for adsorption equilibrium (>30 min). The spectra of the adsorbed species on the WO_3 nanoparticles were obtained by subtracting the background spectrum from the sample spectrum. No visible effect was observed in the ATR-FTIR measurements of the cast WO_3 thin film for slight dissolution/dispersion of WO_3 nanoparticles.

On the other hand, the spectra of the dissolved Phe, Phg, or TMβCDx aqueous solution were obtained by subtracting the background spectrum from the sample spectrum at the same pH and ionic strength.

3. RESULTS AND DISCUSSION

3.1. Inclusion Phenomena of TMβCDx with Aromatic α-Amino Acids. An amino acid has both an acidic carboxyl group (−COOH) and a basic amine group (−NH_2) and, therefore, exhibits pH-dependent electrical properties due to protonation/deprotonation of the corresponding functional groups: cationic form [CF] in acidic media, zwitterionic form [ZF] in intermediate media, and anionic form [AF] in basic media.

Bulk aqueous solutions of Phe and Phg show characteristic absorption signals in the UV region of 200−300 nm exclusively due to aromatic side-chains (designated as L_a and L_b band according to Platt's nomenclature[42]). Note that a significant difference between Phe and Phg is the presence or absence of a methylene spacer between the aromatic benzene ring and the chiral α-carbon. The TMβCDx inclusion complexations of Phe and Phg molecules were quantitatively investigated at various pH conditions by UV−vis absorption titration. Typical examples are given in Figure S2 in Supporting Information, which shows the UV absorption spectra of Phe and Phg in the acidic aqueous system containing various concentrations of TMβCDx. As shown in Figure S2a in Supporting Information, the L_b band maximum of Phe (258 nm) was gradually shifted to a longer wavelength upon the addition of TMβCDx. The neutral and basic aqueous systems also showed similar spectral changes (not shown). The red-shift in the absorption band, in addition to the well-defined isosbestic points, was consistent with the inclusion of the aromatic moiety of amino acids into the hydrophobic cyclodextrin inner cavity.[43] In contrast, neither the absorption spectra of Phg at pH range tested showed significant changes in the presence of TMβCDx, even at the high concentrations, probably resulting from a very weak interaction between Phg and TMβCDx molecules. Phg is a relatively rigid molecule with only one rotatable bond. These opposing results are, therefore, likely due to the Phe molecule's greater flexibility than the Phg one, the greater distance between hydrophobic and hydrophilic moieties, and deeper penetration into the TMβCDx hydrophobic cavity.[44]

Generally, the formation of a 1:1 inclusion complex between native β-cyclodextrin (nonfunctionalized) and aromatic compounds has been extensively reported.[45] Since the Phe molecule has two acidic dissociation constants (K_{a1} and K_{a2}) of the carboxyl and amine groups, respectively, we will consider three stability constants for three different forms (CF, ZF, and AF). Also, assuming the formation of 1:1 TMβCDx-complexed CF, ZF, and AF of Phe in the present systems, we analyzed herein the observed absorption spectral data in the L_b band region by means of modified Benesi−Hildebrand-type equation containing acid dissociation constants for Phe. Herein, a double reciprocal plot can be used to more accurately determine stability constants for TMβCDx-complexed Phe molecules with the change in absorbance as a function of concentration of proton, Phe, and TMβCDx (eq 3)

Table 2. Stability Constants of 1:1 TMβCDx-Complexed AA Molecules in Aqueous Solution, Saturated Concentrations, and Adsorption Constants of AA and TMβCDx-Complexed AA Molecules onto the WO_3 Nanocolloid Surface at 25 °C

		ion strength[a]/mol dm^{-3}	aromatic α-amino acid	
			Phg	Phe
binding constants/mol dm^3	K_{cpx_CF}	0.1		$(0.18 \pm 0.05) \times 10^2$
	K_{cpx_ZF}	0.1		$(0.11 \pm 0.03) \times 10^2$
	K_{cpx_AF}	0.1		$(1.01 \pm 0.14) \times 10^2$
saturated conc./mol dm^{-2}	a_{AA}	0.01−0.1	$(2.81 \pm 0.21) \times 10^{-8}$	$(2.51 \pm 0.13) \times 10^{-8}$
	$a_{AA\text{-}CDx}$	0.01−0.1		$(0.81 \pm 0.09) \times 10^{-8}$
adsorption constant/dm	K_{CF}'	0.01	$(9.98 \pm 0.47) \times 10^{-4}$	$(7.97 \pm 0.38) \times 10^{-4}$
		0.05	$(8.21 \pm 0.40) \times 10^{-4}$	$(6.18 \pm 0.33) \times 10^{-4}$
		0.1	$(6.12 \pm 0.31) \times 10^{-4}$	$(5.38 \pm 0.29) \times 10^{-4}$
	K_{ZF}'	0.01	$(9.71 \pm 0.35) \times 10^{-6}$	$(9.52 \pm 0.33) \times 10^{-6}$
		0.05	$(8.05 \pm 0.38) \times 10^{-6}$	$(7.44 \pm 0.27) \times 10^{-6}$
		0.1	$(5.89 \pm 0.32) \times 10^{-6}$	$(5.08 \pm 0.25) \times 10^{-6}$
	K_{AF}'	0.01	not obtained	not obtained
		0.05	not obtained	not obtained
		0.1	not obtained	not obtained
	$K_{CF\text{-}CDx}'$	0.01		$(1.10 \pm 0.21) \times 10^{-2}$
		0.05		$(1.14 \pm 0.23) \times 10^{-2}$
		0.1		$(1.09 \pm 0.18) \times 10^{-2}$
	$K_{ZF\text{-}CDx}'$	0.01		$(8.32 \pm 0.78) \times 10^{-4}$
		0.05		$(7.99 \pm 0.66) \times 10^{-4}$
		0.1		$(8.17 \pm 0.72) \times 10^{-4}$
	$K_{AF\text{-}CDx}'$	0.01		not obtained
		0.05		not obtained
		0.1		not obtained

[a]Ion strength was kept with sodium sulfate.

$$\begin{aligned}\frac{1}{\mathrm{Abs}-\mathrm{Abs}_{\mathrm{ini}}} &= \frac{K_{a1}K_{a2}+K_{a1}[\mathrm{H}^+]+[\mathrm{H}^+]^2}{\Delta\varepsilon[\mathrm{H}^+]^2[\mathrm{Phe}]} \\ &+ \frac{K_{a1}K_{a2}+K_{a1}[\mathrm{H}^+]+[\mathrm{H}^+]^2}{\Delta\varepsilon K_{a1}[\mathrm{H}^+][\mathrm{Phe}]} \\ &+ \frac{K_{a1}K_{a2}+K_{a1}[\mathrm{H}^+]+[\mathrm{H}^+]^2}{\Delta\varepsilon K_{a1}K_{a2}[\mathrm{Phe}]} \\ &+ \frac{K_{a1}K_{a2}+K_{a1}[\mathrm{H}^+]+[\mathrm{H}^+]^2}{K_{cpx\_CF}[\mathrm{TM}\beta\mathrm{CDx}]\Delta\varepsilon[\mathrm{H}^+]^2[\mathrm{Phe}]} \\ &+ \frac{K_{a1}K_{a2}+K_{a1}[\mathrm{H}^+]+[\mathrm{H}^+]^2}{K_{cpx\_ZF}[\mathrm{TM}\beta\mathrm{CDx}]\Delta\varepsilon K_{a1}[\mathrm{H}^+][\mathrm{Phe}]} \\ &+ \frac{K_{a1}K_{a2}+K_{a1}[\mathrm{H}^+]+[\mathrm{H}^+]^2}{K_{cpx\_AF}[\mathrm{TM}\beta\mathrm{CDx}]\Delta\varepsilon K_{a1}K_{a2}[\mathrm{Phe}]}\end{aligned} \quad (3)$$

where Abs and $\mathrm{Abs_{ini}}$ are the absorbance in the presence and absence of TMβCDx, respectively. [TMβCDx] and [Phe] refer to the initial concentration of TMβCDx and Phe, respectively. That means, by definition, [Phe] = ([CF] + [ZF] + [AF]). $\Delta\varepsilon$ denotes the change in the molar extinction coefficient between the free and complexed Phe. K_{cpx_CF}, K_{cpx_ZF}, and K_{cpx_AF} are the stability constant for the formation of the 1:1 TMβCDx-complexed CF, ZF, and AF of Phe, respectively, and are defined as follows

$$K_{cpx\_CF} = \frac{[\mathrm{TM}\beta\mathrm{CDx}\cdot\mathrm{CF}]}{[\mathrm{TM}\beta\mathrm{CDx}][\mathrm{CF}]} \quad (4)$$

$$K_{cpx\_ZF} = \frac{[\mathrm{TM}\beta\mathrm{CDx}\cdot\mathrm{ZF}]}{[\mathrm{TM}\beta\mathrm{CDx}][\mathrm{ZF}]} \quad (5)$$

$$K_{cpx\_AF} = \frac{[\mathrm{TM}\beta\mathrm{CDx}\cdot\mathrm{AF}]}{[\mathrm{TM}\beta\mathrm{CDx}][\mathrm{AF}]} \quad (6)$$

where [TMβCDx·CF], [TMβCDx·ZF], and [TMβCDx·AF] denote the concentration of TMβCDx-complexed CF, ZF, and AF of Phe, respectively. Equation 3 holds under the experimental conditions of a higher concentration of TMβCDx than that of Phe (at least 10 times). A plot of 1/Abs−$\mathrm{Abs_{ini}}$ versus 1/[TMβCDx] gives a linear relationship at various pHs, as shown in Figure S3 in Supporting Information. The stability constants of each TMβCDx complex were calculated from the slope and the intercept of the plots and given in Table 2. The TMβCDx inclusion behavior was distinctly different for each of the Phe molecule's three forms (CF, ZF, and AF). Under the buffered neutral aqueous condition where Phe molecules ionized as zwitterions, the tendency to form inclusion complexes was relatively lower than those observed under acidic and basic aqueous ones. This trend has also been reported for the native β-cyclodextrin-complexed α-amino acids in aqueous media.[46]

3.2. Adsorption Isotherm of Aromatic α-Amino Acid on the WO_3 Nanocolloid Surface in the Absence/Presence of TMβCDx. In the aqueous media, under-coordinated metal ions on the top layer of metal oxide surfaces react more readily with water molecules to form surface hydroxyl groups to complete their coordination sphere. Thus, the specific protonation/deprotonation of the resulting surface hydroxyl groups brings about pH-dependent charges on the surface of metal oxides.[47] The surface charge state of metal oxide particles can be understood with the knowledge of

https://doi.org/10.1021/acsomega.3c09239
ACS Omega 2024, 9, 18957−18972

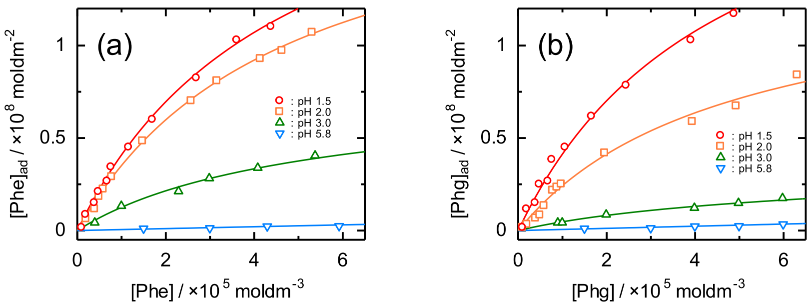

Figure 1. Adsorption isotherms of (a) Phe and (b) Phg molecules on the WO_3 colloid surface at various pH values. The solid line is the best-fitting data for eq 7 (see text). Concentration conditions: [AA] = 1.0 × 10^{-4} M, [WO_3] = 1.0 × 10^{-6} to 5.0 × 10^{-2} M, [Na_2SO_4] = 3.3 × 10^{-2} M.

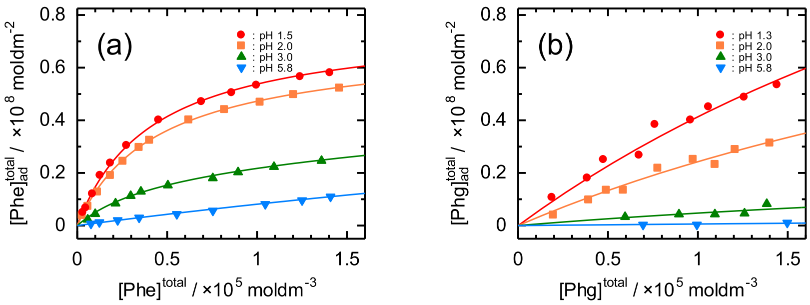

Figure 2. Adsorption isotherms of (a) Phe and (b) Phg molecules on the WO_3 colloid surface in the presence of TMβCDx molecules at various pH values. The solid lines are the best fit of data to eq 11 (see text). Concentration conditions: [AA] = 1.0 × 10^{-4} M, [TMβCDx] = 1.0 × 10^{-2} M, [WO_3] = 1.0 × 10^{-6} to 5.0 × 10^{-2} M, [Na_2SO_4] = 3.3 × 10^{-2} M.

the PZC at a pH where they carry a zero net charge. Charged metal oxide surfaces attract and hold ionic species more strongly than nonionic ones.[40]

A detailed adsorption analysis of AAs on the WO_3 nanocolloid particles will provide us insight into intrinsic interaction pathways on the nanostructured surface. The concentrations of AAs adsorbed on the surface of WO_3 particles were also determined using HPLC technique. The results in the AA/WO_3 binary and AA/TMβCDx/WO_3 ternary aqueous system at various pHs are presented in Figures 1 and 2, respectively. The pH value remarkably influences AAs' adsorption behavior, regardless of the presence or absence of TMβCDx. In acidic media, the measured isotherm shows a sharp initial rise, while the plots gradually change at neutral pH. Notably, the presence of TMβCDx remarkably promotes the adsorptivity of Phe molecules onto WO_3 particles. The shape of each set of adsorption isotherms has a clear Langmuir-type plateau, thereby clearly indicating the applicability of a monolayer coverage of AAs' species on the WO_3 surface. Although the Langmuir isotherm has been used to resolve the molecular adsorption mechanism at surfaces, this isotherm model is not highly applicable because three equilibrated forms (CF, ZF, and AF) of AAs would be present in both binary and ternary systems (see Figure S1a,b in Supporting Information for details). In order to analyze the adsorption behavior of AAs onto the WO_3 colloid surface, we used the following modified Langmuir isotherm equation in the AA/WO_3 binary aqueous system

$$[\mathrm{AA}]_{\mathrm{ad}} = \frac{a_{\mathrm{AA}}K'_{\mathrm{CF}}[\mathrm{H}^+]^2[\mathrm{AA}]}{a_{\mathrm{AA}}(K_{\mathrm{a1}}K_{\mathrm{a2}} + K_{\mathrm{a1}}[\mathrm{H}^+] + [\mathrm{H}^+]^2) + K'_{\mathrm{CF}}[\mathrm{H}^+]^2[\mathrm{AA}]} + \frac{aK'_{\mathrm{ZF}}K_{\mathrm{a1}}[\mathrm{H}^+][\mathrm{AA}]}{a_{\mathrm{AA}}(K_{\mathrm{a1}}K_{\mathrm{a2}} + K_{\mathrm{a1}}[\mathrm{H}^+] + [\mathrm{H}^+]^2) + K'_{\mathrm{ZF}}K_{\mathrm{a1}}[\mathrm{H}^+][\mathrm{AA}]} + \frac{aK'_{\mathrm{AF}}K_{\mathrm{a1}}K_{\mathrm{a2}}[\mathrm{AA}]}{a_{\mathrm{AA}}(K_{\mathrm{a1}}K_{\mathrm{a2}} + K_{\mathrm{a1}}[\mathrm{H}^+] + [\mathrm{H}^+]^2) + K'_{\mathrm{AF}}K_{\mathrm{a1}}K_{\mathrm{a2}}[\mathrm{AA}]} \quad (7)$$

In this equation, the first, second, and third algebraic fractions on the right-hand side represent the Langmuir-type adsorption of CF, ZF, and AF, respectively, of AAs. $[\mathrm{AA}]_{\mathrm{ad}}$ and [AA] denote the concentration of AA on the WO_3 colloid surface (mol dm^{-2}) and that in the aqueous solution (mol dm^{-3}), respectively. Herein, a_{AA} and $[\mathrm{H}^+]$ refer to the saturated concentration of AA on the WO_3 colloid surface (mol dm^{-2}) and the concentration of proton in the aqueous solution (mol dm^{-3}), respectively. K'_{CF}, K'_{ZF}, and K'_{AF}, respectively, are the adsorption constants of CF, ZF, and AF of AA onto the WO_3 colloid surface and are defined as follows

$$K'_{\mathrm{CF}} = \frac{[\mathrm{CF}]_{\mathrm{ad}}}{[\mathrm{CF}]} \quad (8)$$

$$K'_{\mathrm{ZF}} = \frac{[\mathrm{ZF}]_{\mathrm{ad}}}{[\mathrm{ZF}]} \quad (9)$$

$$K'_{\mathrm{AF}} = \frac{[\mathrm{AF}]_{\mathrm{ad}}}{[\mathrm{AF}]} \quad (10)$$

where the brackets with and without subscript "ad" denote the concentration of each form on the WO_3 colloid surface (mol dm^{-2}) and in the aqueous solution (mol dm^{-3}), respectively. That means, by definition, $[\mathrm{AA}]_{\mathrm{ad}} = ([\mathrm{CF}]_{\mathrm{ad}} + [\mathrm{ZF}]_{\mathrm{ad}} + [\mathrm{AF}]_{\mathrm{ad}})$ and $[\mathrm{AA}] = ([\mathrm{CF}] + [\mathrm{ZF}] + [\mathrm{AF}])$.

https://doi.org/10.1021/acsomega.3c09239
ACS Omega 2024, 9, 18957−18972

In the Phe/TMβCDx/WO_3 ternary aqueous system, it is important to consider how the free TMβCDx molecules, the three charged forms of Phe molecules, and the corresponding TMβCDx complexes are adsorbed onto the surface. Since the adsorptivity of TMβCDx molecules on WO_3 nanocolloid particles is actually negligibly small (see SI-2 section in Supporting Information), the competitive adsorption model between free Phe and TMβCDx-complexed Phe molecules can explain the adsorption behavior in the ternary system. The isotherm equation in this ternary system was further modified to include the stability constant term of the TMβCDx complexes as the following

$$
\begin{aligned}
[\mathrm{Phe}]_{\mathrm{ad}}^{\mathrm{total}} = {} & \frac{a_{\mathrm{AA}}K'_{\mathrm{CF}}[\mathrm{H}^+]^2[\mathrm{Phe}]^{\mathrm{total}}}{a_{\mathrm{AA}}(K_{\mathrm{a1}}K_{\mathrm{a2}} + K_{\mathrm{a1}}[\mathrm{H}^+] + [\mathrm{H}^+]^2) + K'_{\mathrm{CF}}[\mathrm{H}^+]^2[\mathrm{Phe}]^{\mathrm{total}}} \\
& + \frac{a_{\mathrm{AA}}K'_{\mathrm{ZF}}K_{\mathrm{a1}}[\mathrm{H}^+][\mathrm{Phe}]^{\mathrm{total}}}{a_{\mathrm{AA}}(K_{\mathrm{a1}}K_{\mathrm{a2}} + K_{\mathrm{a1}}[\mathrm{H}^+] + [\mathrm{H}^+]^2) + K'_{\mathrm{ZF}}K_{\mathrm{a1}}[\mathrm{H}^+][\mathrm{Phe}]^{\mathrm{total}}} \\
& + \frac{a_{\mathrm{AA}}K'_{\mathrm{AF}}K_{\mathrm{a1}}K_{\mathrm{a2}}[\mathrm{Phe}]^{\mathrm{total}}}{a_{\mathrm{AA}}(K_{\mathrm{a1}}K_{\mathrm{a2}} + K_{\mathrm{a1}}[\mathrm{H}^+] + [\mathrm{H}^+]^2) + K'_{\mathrm{AF}}K_{\mathrm{a1}}K_{\mathrm{a2}}[\mathrm{Phe}]^{\mathrm{total}}} \\
& + \frac{a_{\mathrm{AA\text{-}CDx}}K'_{\mathrm{CF\text{-}CDx}}K_{\mathrm{cpx\_CF}}[\mathrm{H}^+]^2[\mathrm{TM}\beta\mathrm{CDx}][\mathrm{Phe}]^{\mathrm{total}}}{a_{\mathrm{AA\text{-}CDx}}(K_{\mathrm{a1}}K_{\mathrm{a2}} + K_{\mathrm{a1}}[\mathrm{H}^+] + [\mathrm{H}^+]^2) + K'_{\mathrm{CF\text{-}CDx}}K_{\mathrm{cpx\_CF}}[\mathrm{H}^+]^2[\mathrm{TM}\beta\mathrm{CDx}][\mathrm{Phe}]^{\mathrm{total}}} \\
& + \frac{a_{\mathrm{AA\text{-}CDx}}K'_{\mathrm{ZF\text{-}CDx}}K_{\mathrm{a1}}K_{\mathrm{cpx\_ZF}}[\mathrm{H}^+][\mathrm{TM}\beta\mathrm{CDx}][\mathrm{Phe}]^{\mathrm{total}}}{a_{\mathrm{AA\text{-}CDx}}(K_{\mathrm{a1}}K_{\mathrm{a2}} + K_{\mathrm{a1}}[\mathrm{H}^+] + [\mathrm{H}^+]^2) + K'_{\mathrm{ZF\text{-}CDx}}K_{\mathrm{a1}}K_{\mathrm{cpx\_ZF}}[\mathrm{H}^+][\mathrm{TM}\beta\mathrm{CDx}][\mathrm{Phe}]^{\mathrm{total}}} \\
& + \frac{a_{\mathrm{AA\text{-}CDx}}K'_{\mathrm{AF\text{-}CDx}}K_{\mathrm{a1}}K_{\mathrm{a2}}K_{\mathrm{cpx\_AF}}[\mathrm{TM}\beta\mathrm{CDx}][\mathrm{Phe}]^{\mathrm{total}}}{a_{\mathrm{AA\text{-}CDx}}(K_{\mathrm{a1}}K_{\mathrm{a2}} + K_{\mathrm{a1}}[\mathrm{H}^+] + [\mathrm{H}^+]^2) + K'_{\mathrm{AF\text{-}CDx}}K_{\mathrm{a1}}K_{\mathrm{a2}}K_{\mathrm{cpx\_AF}}[\mathrm{TM}\beta\mathrm{CDx}][\mathrm{Phe}]^{\mathrm{total}}}
\end{aligned}
\tag{11}
$$

On the right-hand side of the equation, the first three algebraic fractions correspond to the Langmuir-type adsorption of free Phe molecules, while the last three correspond to the same for TMβCDx-complexed Phe molecules. Herein, $a_{\mathrm{AA\text{-}CDx}}$ is the saturated concentration of TMβCDx-complexed Phe molecules on the WO_3 colloid surface (mol dm^{-2}) $K'_{\mathrm{CDx\text{-}CF}}$, $K'_{\mathrm{CDx\text{-}ZF}}$, and $K'_{\mathrm{CDx\text{-}AF}}$, respectively, are the adsorption constants of the 1:1 TMβCDx-complexed CF, ZF, and AF of Phe molecules onto the WO_3 colloid surface, and are defined as follows

$$K'_{\mathrm{CDx\text{-}CF}} = \frac{[\mathrm{TM}\beta\mathrm{CDx}\cdot\mathrm{CF}]_{\mathrm{ad}}}{[\mathrm{TM}\beta\mathrm{CDx}\cdot\mathrm{CF}]} \tag{12}$$

$$K'_{\mathrm{CDx\text{-}ZF}} = \frac{[\mathrm{TM}\beta\mathrm{CDx}\cdot\mathrm{ZF}]_{\mathrm{ad}}}{[\mathrm{TM}\beta\mathrm{CDx}\cdot\mathrm{ZF}]} \tag{13}$$

$$K'_{\mathrm{CDx\text{-}AF}} = \frac{[\mathrm{TM}\beta\mathrm{CDx}\cdot\mathrm{AF}]_{\mathrm{ad}}}{[\mathrm{TM}\beta\mathrm{CDx}\cdot\mathrm{AF}]} \tag{14}$$

Herein, that means, by definition, $[\mathrm{Phe}]_{\mathrm{ad}}^{\mathrm{total}} = ([\mathrm{CF}]_{\mathrm{ad}} + [\mathrm{ZF}]_{\mathrm{ad}} + [\mathrm{AF}]_{\mathrm{ad}} + [\mathrm{TM}\beta\mathrm{CDx}\cdot\mathrm{CF}]_{\mathrm{ad}} + [\mathrm{TM}\beta\mathrm{CDx}\cdot\mathrm{ZF}]_{\mathrm{ad}} + [\mathrm{TM}\beta\mathrm{CDx}\cdot\mathrm{AF}]_{\mathrm{ad}})$ and $[\mathrm{Phe}]^{\mathrm{total}} = ([\mathrm{CF}] + [\mathrm{ZF}] + [\mathrm{AF}] + [\mathrm{TM}\beta\mathrm{CDx}\cdot\mathrm{CF}] + [\mathrm{TM}\beta\mathrm{CDx}\cdot\mathrm{ZF}] + [\mathrm{TM}\beta\mathrm{CDx}\cdot\mathrm{AF}])$ (see Scheme S1 in Supporting Information in for various equilibria in this ternary aqueous system). The adsorption parameters derived from the least-squares curve-fitting analysis of eqs 7 or 11 under various pH conditions are summarized in Table 2. Note that K'_{AF} and $K'_{\mathrm{AF\text{-}CDx}}$ values were unable to be obtained, because the concentration of AF was extremely smaller under the pH range of 1−6. Since the determined PZC value of the as-prepared WO_3 is about 0.2, the surface charge of the WO_3 particles is always negative under the pH conditions (see Section 2.2 and Figure S9 in Supporting Information).

In the AA/WO_3 binary aqueous system, the K'_{CF} values for both Phe and Phg molecules are significantly larger than the K'_{ZF} values found for the corresponding amino acid (see Table 2), indicating the high affinity between the CF and the WO_3 particle surface. Using the observed saturated concentration (a) values of Phe and Phg in the binary aqueous system, the area per molecule on the WO_3 surface was calculated to be 83 and 77 Å^2 per molecule, respectively. The projection area of Phe and Phg is estimated to be ca. 70−90 Å^2 from the calculated CPK model. Therefore, it is evident that both Phe and Phg molecules are adsorbed relatively densely on the surface of WO_3 particles. Moreover, to further delineate the adsorption characteristics of Phe and Phg onto the WO_3 colloid surface, we set out to quantify the influence of ionic strength on the isotherm under a constant concentration of corresponding amino acid. Evaluating adsorption as a function of ionic strength can provide insight into the long-range electrostatic forces and near-range physical and chemical forces involved in molecular adsorption. As listed in Table 2, Phe and Phg's adsorption constants decreased with increasing ionic strength (salt concentration). This finding reveals that electrostatic interaction between the positively charged amino group of Phe and Phg molecules and the negatively charged WO_3 surface is the critical factor governing the adsorption behavior on the WO_3 colloid surface.

The adsorption parameters in the Phe/TMβCDx/WO_3 ternary aqueous system are also calculated using experimental dependences on the pH and ionic strength. It is herein intriguing that the molecular occupied area of the TMβCDx-complexed Phe molecule determined from the saturated surface concentration values of Langmuir model in the ternary aqueous system is approximately equal to the vertical sectional area of the TMβCDx molecule against the C_7 axis (213 Å^2), revealing a steric role of the TMβCDx in the adsorption

https://doi.org/10.1021/acsomega.3c09239
ACS Omega 2024, 9, 18957−18972

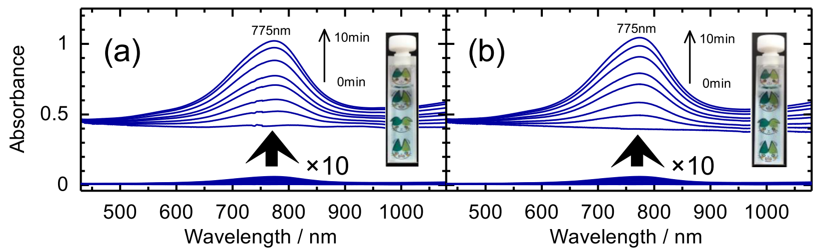

Figure 3. Typical absorption spectral changes of (a) as-prepared WO_3 and (b) TMβCDx/WO_3 binary aqueous solution under UV light irradiation. Concentration conditions: $[WO_3] = 1.0 \times 10^{-2}$ M, [TMβCDx] $= 1.0 \times 10^{-2}$ M, $[Na_2SO_4] = 3.3 \times 10^{-2}$ M, pH 1.5. The insets show the photograph of the sample solutions after the irradiation for 30 min.

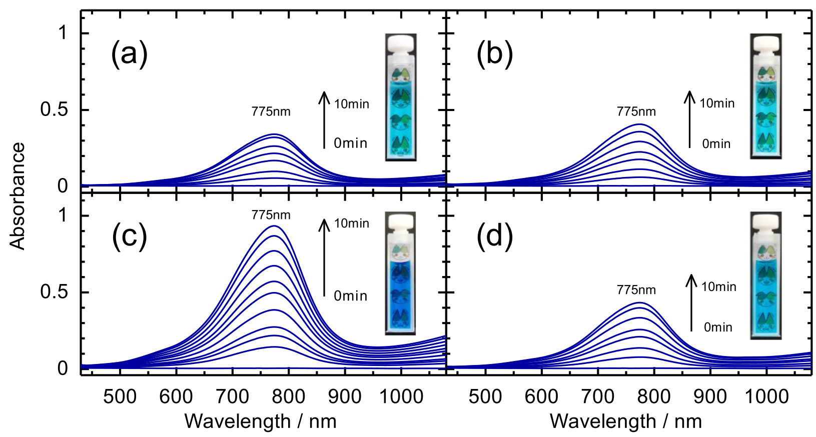

Figure 4. Typical absorption spectral changes of (a) Phe/WO_3 binary (b) Phg/WO_3 binary, (c) Phe/TMβCDx/WO_3 ternary, and (d) Phg/TMβCDx/WO_3 ternary aqueous solution under UV light irradiation. Concentration conditions: $[WO_3] = 1.0 \times 10^{-2}$ M, [AA] $= 1.0 \times 10^{-3}$ M, [TMβCDx] $= 1.0 \times 10^{-2}$ M, $[Na_2SO_4] = 3.3 \times 10^{-2}$ M, pH 1.5. The insets show the photograph of the sample solutions after the irradiation for 10 min.

process of TMβCDx-complexed Phe onto the WO_3 surface. Moreover, the adsorption constants of the TMβCDx inclusion complex of Phe obtained in the Phe/TMβCDx/WO_3 ternary aqueous system are about 2 orders of magnitude larger than those of the corresponding free (unincluded) Phe. Namely, the adsorptivity of Phe molecules onto the WO_3 particles was remarkably promoted due to the formation of inclusion complexes in the aqueous media. As is evident from Figure 2 and Table 2, the adsorptivity of TMβCDx·CF inclusion complexes of Phe molecules on WO_3 is also much higher than that of the corresponding TMβCDx·ZF ones, which is similar to the adsorption trend of free aromatic amino acids on the WO_3 surface as described above. Note that the adsorption constants of the TMβCDx-complexed Phe molecules were completely independent of the ionic strength. The different adsorption isotherms in the binary and ternary aqueous systems may stem from the difference in the two adsorption modes of Phe molecules on the WO_3 surface sites. We will discuss the characterization of the multiple adsorption modes of AAs in a later section.

3.3. Kinetic Analysis of Photochromic Behaviors in Aromatic α-Amino Acid/WO_3 Binary and Aromatic α-Amino Acid/TMβCDx/WO_3 Ternary Aqueous System.

The AA/WO_3 binary and AA/TMβCDx/WO_3 ternary aqueous solutions were stable without precipitate for a week at room temperature. Indeed, the TEM result showed that no agglomeration of the WO_3 nanocolloid particles occurred by the addition of AAs and/or TMβCDx (see Figure S8 in Supporting Information). It is of great importance for chromic probe materials to be well dissolved/dispersed in any aqueous systems to move toward realistic implementation.

We investigated the photochromic behaviors of the AA/WO_3 binary and AA/TMβCDx/WO_3 ternary aqueous solutions under UV irradiation. Initially, the photochromism in the WO_3 unary and TMβCDx/WO_3 binary aqueous system was preliminary examined. Both as-prepared WO_3 and TMβCDx/WO_3 binary aqueous solutions have an optical band gap of 386 nm (3.21 eV), which is consistent with their colorless and transparent feature in the ground state. Under UV excitation where the wavelength of the most intense line was 366 nm, both solutions changed to a light blue color after a few minutes, as detectable by the naked-eye (see inset in Figure 3). This color change is doubtless associated with the formation of bronze-type tungsten oxide compounds caused by partial reduction of tungsten atoms,[48] whose broad absorption band peaking at 775 nm gradually increases with UV irradiation time (Figure 3). The detailed mechanism of photoinduced coloration will be described in a later section. Noted here that the presence/absence of TMβCDx does not affect the UV-induced color change behavior of the WO_3 aqueous solution.

The UV-induced photochromic behaviors of the AA/WO_3 binary and AA/TMβCDx/WO_3 ternary aqueous solutions are also displayed in Figure 4. Interestingly, the AA/WO_3 binary aqueous solutions showed an obvious photochromic effect than the as-prepared WO_3 aqueous one, and the Phe/TMβCDx/WO_3 ternary aqueous ones showed an even more intense enhanced photochromic effect than the corresponding Phe/WO_3 binary aqueous ones. Judging from the photo-

https://doi.org/10.1021/acsomega.3c09239
ACS Omega 2024, 9, 18957−18972

chromic coloration and adsorption isotherm results in the as-prepared WO_3, TMβCDx/WO_3 binary, and AA/WO_3 binary aqueous systems, it can be concluded unambiguously that only the AA molecules adsorbed on the WO_3 surface affects the photochromic properties of the aqueous WO_3 solutions, as we previously pointed out.[28,29] Importantly, no significant enhanced photochromic effect with the addition of TMβCDx was observed in the Phg/TMβCDx/WO_3 ternary aqueous system, where the weak intermolecular interaction between Phg and TMβCDx molecule makes it unlikely to form inclusion complex (see Section 3.1).

Figure 5 shows the time profiles of the absorbance at 775 nm of the AA/WO_3 binary and AA/TMβCDx/WO_3 ternary

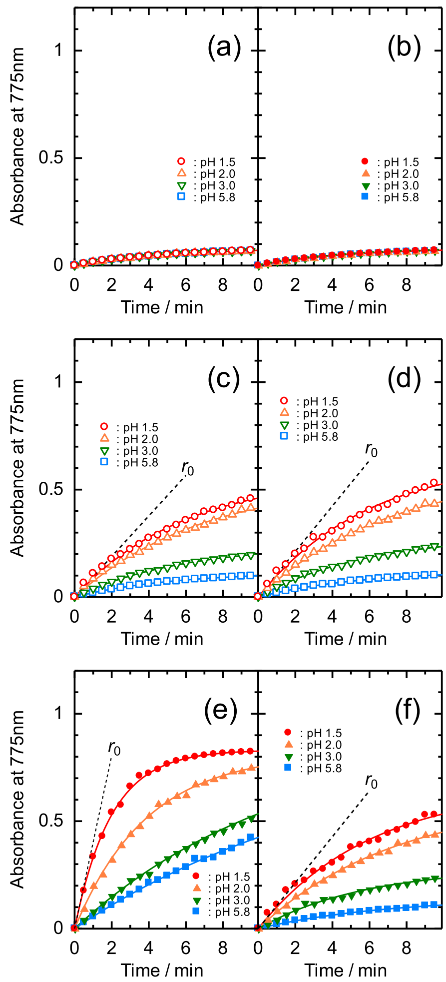

Figure 5. Time profiles of the absorbance at 775 nm of (a) as-prepared WO_3, (b) TMβCDx/WO_3 binary (c) Phe/WO_3 binary, (d) Phg/WO_3 binary (e) Phe/TMβCDx/WO_3 ternary, and (f) Phg/TMβCDx/WO_3 ternary aqueous solution under UV light irradiation at various pH values. Concentration conditions: $[WO_3] = 1.0 \times 10^{-2}$ M, $[TM\beta CDx] = 1.0 \times 10^{-2}$ M, $[Na_2SO_4] = 3.3 \times 10^{-2}$ M.

aqueous solutions under UV light irradiation at various pH values. The coloration kinetics of the as-prepared WO_3 and TMβCDx/WO_3 binary aqueous solutions are also shown in Figure 5 for reference. As indicated in the figure, the initial coloration rate (r_0) of the photochromic behaviors is given by the rate of increase of the absorbance at 775 nm (Abs_{775}) versus the time curve at t = 0.

$$r_0 = \left| \frac{d(Abs_{775})}{dt} \right|_{t=0} \tag{15}$$

The actual values were assessed by differentiating the quadratic equation fitted to the observed points. The r_0 values in the AA/WO_3 binary and AA/TMβCDx/WO_3 ternary aqueous system varied depending on their pH levels, whereas there was no variation in r_0 ones in the as-prepared WO_3 and TMβCDx/WO_3 binary aqueous system. Because the adsorption isotherms of AAs molecules onto the WO_3 particles are essentially dependent on pH, this difference should be ascribable to AAs' forms (CF, ZF, or AF) adsorbed on the WO_3 surface.

We have previously reported the unique surface-enhanced photochromic phenomena, in which the photochromic coloration of inorganic oxide semiconductor particles (such as WO_3 and MoO_3) can be dramatically enhanced by surface-adsorbed organic compounds. Herein, the colorimetric analytical performance based on the surface-enhanced photochromic phenomenon was compared in the absence and presence of TMβCDx, using the initial coloration rate (r_0), which is suitable for rapid and effective monitoring. Figure 6 shows the experimental data for r_0 values as a function of the total concentration of various aromatic amino acids on the

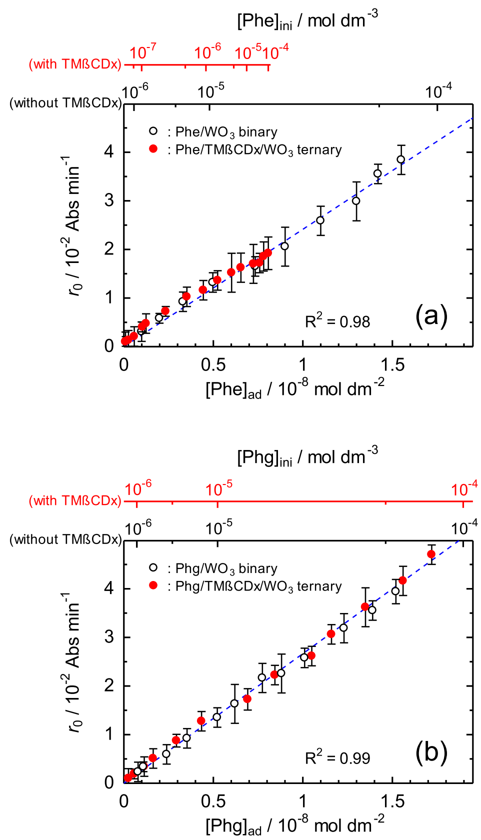

Figure 6. Dependence of the initial coloration rate (r_0) on the concentration of AA adsorbed on the WO_3 colloid surface {(a) $[Phe]_{ad}$ and (b) $[Phg]_{ad}$; lower axis} and the initial concentration of AA {(a) $[Phe]_{ini}$ and (b) $[Phg]_{ini}$; upper axis} in the absence (primary upper axis) and presence (secondary upper axis) of TMβCDx. The straight lines indicate the best-fitting curves obtained by the least-squares method. The magnitude of the error bars was calculated from the uncertainty given by five independent measurements.

https://doi.org/10.1021/acsomega.3c09239
ACS Omega 2024, 9, 18957−18972

WO_3 surface ($[AA]_{ad}$), which was calculated by using the stability and adsorption parameters obtained in this study, i.e., $[AA]_{ad} = [CF]_{ad} + [ZF]_{ad} + [AF]_{ad}$ in the AA/WO_3 binary aqueous system; $[AA]_{ad} = [CF]_{ad} + [ZF]_{ad} + [AF]_{ad} + [CF\text{-}CDx]_{ad} + [ZF\text{-}CDx]_{ad} + [AF\text{-}CDx]_{ad}$ in the AA/TMβCDx/WO_3 ternary aqueous system. The upper axes show the initial bulk concentration of AA in the binary (without TMβCDx) and ternary (with TMβCDx) aqueous system. Error bars of r_0 values denote σ, where σ is a standard deviation from an average of five measurements. As shown in Figure 6, linear relationships between r_0 value and $[AA]_{ad}$ were obtained in the range from ca. 1.0×10^{-10} to 2.0×10^{-8} mol dm^{-2}: for Phe (slope = 2.41×10^6 Abs dm^2 mol^{-1} min^{-1}, $R^2 = 0.98$) and for Phg (slope = 2.67×10^6 Abs dm^2 mol^{-1} min^{-1}, $R^2 = 0.99$). Here, we would like to highlight that the enhanced photochromic phenomenon gives us quantitative information about amino acid molecules that are in direct contact with the WO_3 colloid surface. Comparing the results in the binary aqueous system to ones in the ternary aqueous system, we see that the two data sets of the aromatic amino acids are in good quantitative agreement, which can be described by the same surface concentration-dependent linear equation. These data confirmed the previously reported findings and further a novel role for TMβCDx in the surface-enhanced photochromic phenomena of inorganic oxide semiconductor particles.

The LOD in general analytical methods is simply the lowest amount of analyte in a sample, detectable but not necessarily quantifiable as an absolute value. Meanwhile, the limit of quantification (LOQ) is the lowest amount of analyte in a sample, which can be determined quantitatively with suitable precision and accuracy. According to ISO guidelines provided,[49] the LOD and LOQ values were evaluated for the r_0 data set obtained in various systems using the intercept and standard deviation of the regression line, respectively (Figure 6). The LOD and LOQ values (in mol dm^{-3}) in the AA/WO_3 binary and the AA/TMβCDx/WO_3 ternary systems are listed in Table 3. Compared with previously published methods for

Table 3. LOD and LOQ Values for Aromatic Amino Acids Determination in Various System[a]

aromatic α-amino acid	system	LOD/mol dm^{-3}	LOQ/mol dm^{-3}
Phe	binary	9.88×10^{-7}	2.99×10^{-6}
	ternary	0.317×10^{-7}	0.0961×10^{-6}
Phg	binary	8.27×10^{-7}	2.50×10^{-6}
	ternary	8.05×10^{-7}	2.44×10^{-6}

[a]LOD: limit of detection, LOQ: limit of quantification, binary: AA/WO_3 aqueous solution, ternary: AA/TMβCDx/WO_3 aqueous solution.

Phe detection (see Table 1), our colorimetric method based on the WO_3 surface-enhanced photochromic phenomena shows excellent sensitivity and good LOD values. Remarkably, the presence of TMβCDx improved both LOD and LOQ values for Phe to about 30-fold higher. In contrast, in the Phg/TMβCDx/WO_3 ternary aqueous system, no improvement in the detection and quantification of Phg was observed by the presence of TMβCDx. There is no doubt that the preferential adsorption of TMβCDx-complexed Phe molecules on the WO_3 surface is directly responsible for the improved sensitivity of Phe detection by the surface-enhanced photochromic phenomenon. Although we have not yet optimized conditions for all amino acids and related compounds, this finding supports the idea that supramolecular host−guest interactions can promote analytical sensitivity of "label-free" colorimetric strategies based on the surface-enhanced photochromic phenomena of metal oxide semiconductor nanoparticles for detecting target molecules for detecting target molecules.

3.4. ATR-FTIR Spectroscopy of Aromatic α-Amino Acids Adsorbed on WO_3 Nanocolloid Particles. The adsorption of amino acids and their derivatives on metal oxide surfaces can be classified as the outer-sphere and inner-sphere adsorption modes, governed by electrostatic and covalent interactions, respectively.[50] Outer-sphere adsorption is electrostatically driven when oppositely charged attract each other through solvent-separated species and is essentially reversible. This adsorption mode is typical when adsorbates are greatly affected by changes in ionic strength. On the other hand, inner-sphere adsorption involves the irreversible formation of metal−ligand coordinated bonds and is often preceded by initial outer-sphere adsorption. This adsorption mode is less affected by changes in ionic strength.[51] In this study, the characteristics of the adsorption modes and configurations of AAs were investigated by attenuated total reflection Fourier transform infrared spectroscopy (ATR-FTIR). The spectra recorded using this technique have a remarkable sensitivity to the adsorbed species, thus making it possible to determine the adsorption modes, including the conformation and structural changes of the AAs adsorbed on the surface of the WO_3 nanocolloid particles.[52]

ATR-FTIR spectra of AAs dissolved in aqueous solution and adsorbed on WO_3 particles deposited on the surface of horizontal ATR crystal in the presence/absence of TMβCDx were collected (Figures 7 and 8). The measurements were

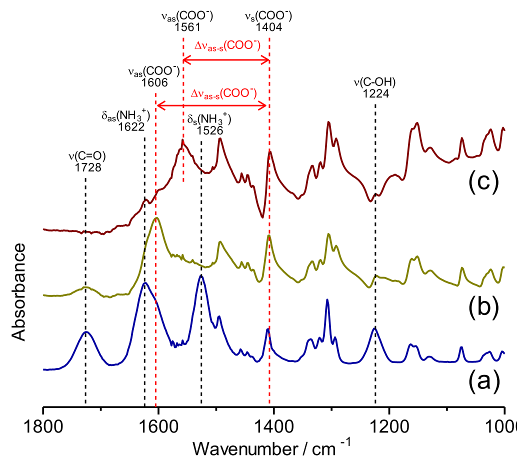

Figure 7. A comparison between ATR-FTIR spectra for (a) acidic Phe aqueous solution, (b) Phe adsorbed on the WO_3 nanoparticles in the absence of TMβCDx, and (c) Phe adsorbed on the WO_3 nanoparticles in the presence of TMβCDx. Concentration conditions: [Phe] = 1.0×10^{-4} M, [TMβCDx] = 1.0×10^{-2} M, [Na_2SO_4] = 3.3×10^{-2} M, pH = 1.5.

conducted only under acidic conditions (pH 1.5), where the most prominent coloration phenomena were observed upon UV irradiation. Characteristic IR absorption bands from various vibration modes of Phe and Phg molecules appeared from 1800 to 1000 cm^{-1} in the wavenumber range. These observed bands were tentatively assigned by referring to several published studies on IR spectra of adsorbed amino acids and related compound molecules (see Table 4).[53−56] Since Phg

https://doi.org/10.1021/acsomega.3c09239
ACS Omega 2024, 9, 18957−18972

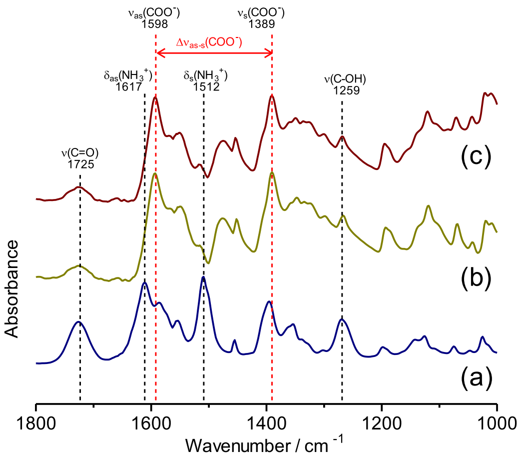

Figure 8. A comparison between ATR-FTIR spectra for (a) acidic Phg aqueous solution, (b) Phg adsorbed on the WO_3 nanoparticles in the absence of TMβCDx, and (c) Phg adsorbed on the WO_3 nanoparticles in the presence of TMβCDx. Concentration conditions: [Phg] = 1.0×10^{-4} M, [TMβCDx] = 1.0×10^{-2} M, [Na_2SO_4] = 3.3×10^{-2} M, pH = 1.5.

and Phe have similar molecular structures, the only difference being the addition of a methylene bridge (−CH_2−) in Phe between the aromatic ring and the polar amino/carboxy groups, it is helpful to compare the corresponding spectra between Phg and Phe.

First, let us analyze the ATR-FTIR spectra of Phe and Phg dissolved in the acidic aqueous solutions (pH 1.5), as shown in Figures 7a and 8a, respectively. For Phe, the prominent bands at 1728, 1622, 1526, 1405, 1321, and 1224 cm^{-1} correspond to C═O stretching vibration [$\nu(C{=}O)_{\text{carboxylic acid}}$] of the carboxyl group (−COOH), asymmetric bending vibration [$\delta_{as}(NH_3^+)$] and symmetric bending vibration [$\delta_s(NH_3^+)$] of the protonated amino group, symmetric vibration [$\nu_s(COO^-)$] of the deprotonated carboxyl group (carboxylate: $-COO^-$), out-of-plane wag vibration [$\omega(CH_2)$] of methylene bridge, and C−OH stretching vibration [$\nu(C{-}OH)_{\text{carboxylic acid}}$] of the carboxyl group, respectively. Also, there was a weak shoulder band at about 1600 cm^{-1}, which was observed as a contribution of asymmetric stretching vibration [$\nu_{as}(COO^-)$] of the carboxylate. For Phg, there was no significant difference in band position from that of Phe in the acidic aqueous solution except for the absence of $\omega(CH_2)$ band. The spectral analysis showed that cationic and zwitterionic species of Phe and Phg are present in this acidic aqueous solution. This result seems reasonable since approximately 74 and 83% of the species distribution of Phg and Phe, respectively, at pH = 1.5 are cationic, while the remaining (26 and 17%) are zwitterionic, based on the corresponding pK_a values (see Scheme 1 and Figure S1 in Supporting Information).[57]

Infrared spectra of Phg and Phe molecules adsorbed on a WO_3 nanocolloid particle film cast on an ATR crystal under acidic conditions (pH = 1.5) are shown in Figures 7b and 8b, respectively. The spectra of AAs adsorbed on the WO_3 nanoparticle film are significantly different from those in the same pH aqueous solution regarding relative band intensities and wavenumbers. These changes are attributed to the interaction between the adsorption sites on the WO_3 surface and the functional groups of AAs. Upon adsorption to WO3, the intensity of $\nu(C{=}O)_{\text{carboxylic acid}}$ band (1728 cm^{-1} for Phe, 1725 cm^{-1} for Phg) and $\nu(C{-}OH)_{\text{carboxylic acid}}$ band (1224 cm^{-1} for Phe, 1259 cm^{-1} for Phg) decreased, while the band intensity of $\nu_{as}(COO^-)$ and $\nu_s(COO^-)$ increased (1606 and 1404 cm^{-1} for Phe, 1598 and 1389 cm^{-1} for Phg, respectively). In addition, the $\delta_{as}(NH_3^+)$ and $\delta_s(NH_3^+)$ bands (1622 and 1526 cm^{-1} for Phe, 1617 and 1515 cm^{-1} for Phg, respectively) were observed to weaken or disappear. These changes can be explained by the consideration that the adsorption occurs via the deprotonated carboxyl group of Phg and Phe molecules, leading to the loss of the double bonding character of the C═O bond and the breakage of some hydrogen bonds of the protonated amino group.[58] Such changes in the contribution of carboxyl and amino groups of Phe and Phg molecules to the IR spectra provide complementary information on structural changes accompanying adsorption to WO_3 particle film.

We also analyzed the ATR-FTIR spectra of Phg and Phe molecules adsorbed to the WO_3 surface in the presence of TMβCDx. Note that the characteristic IR absorption bands of nonadsorbed TMβCDx on WO_3 in the acidic aqueous media are mainly located in the 800−1200 cm^{-1} range, so there is no overlap with amino acid compounds' characteristic absorption bands (1200−1800 cm^{-1}), as shown in the preliminary experiment (Figure S10 in Supporting Information). Therefore, the presence of TMβCDx does not significantly affect the analysis of the adsorption modes and configurations of AAs using the spectra.[59] The ATR-FTIR spectra of Phg molecules on the WO_3 surface in the presence and absence of TMβCDx are very similar, with no significant difference in the band shape or peak position. On the other hand, adsorbed Phe molecules in the presence of TMβCDx show significantly different spectra in terms of relative band intensities [complete disappearance of bands at 1728 cm^{-1} [$\nu(C{=}O)_{\text{carboxylic acid}}$]

Table 4. Peak Positions and Functional Group Assignments for Phe and Phg in Acidic Aqueous Solution and Adsorbed on WO_3 Nanocolloid Particles' Film in the AA/WO_3 Binary and AA/TMβCDx/WO_3 Ternary Aqueous System

peak position/cm^{-1} [a]						
L-phenylalanine (Phe)			L-2-phenylglycine (Phg)			
solution	adsorbed (binary)	adsorbed (ternary)	solution	adsorbed (binary)	adsorbed (ternary)	vibrational modes [b]
1728	1728		1725	1725	1725	$\nu(C{=}O)_{\text{carboxylic acid}}$
1622	1622 (sh)	1622 (sh)	1617	1617 (sh)	1617 (sh)	$\delta_{as}(NH_3^+)$
1600 (sh)	1606	1561	1596 (sh)	1598	1598	$\nu_{as}(COO^-)$
1526			1512	1515 (sh)	1515 (sh)	$\delta_s(NH_3^+)$
1405	1404	1404	1393	1389	1389	$\nu_s(COO^-)$
1321	1321	1321				$\omega(CH_2)$
1224	1224		1259	1259	1259	$\nu(C{-}OH)_{\text{carboxylic acid}}$

[a]sh: shoulder band. [b]ν_s/ν_{as}: symmetric/asymmetric stretches; δ_s/δ_{as}: symmetric/asymmetric bends; and ω: wag vibrations.

https://doi.org/10.1021/acsomega.3c09239
ACS Omega 2024, 9, 18957−18972

and 1224 cm^{-1} [ν(C−OH)$_{carboxylic\ acid}$)] and wavenumbers [peak shift at 1606 cm^{-1} to 1561 cm^{-1} (ν_{as}(COO^-))] from adsorbed ones in the absence of TMβCDx, denoting the difference in the adsorption configuration of free Phe and TMβCDx-complexed Phe molecules on WO_3 surface.

There are three modes of coordination between COO^- group and metal cation: monodentate, bidentate, and bidentate bridging.[60,61] In bidentate coordination, the metal cation interacts with both oxygen atoms of COO^- group, while in monodentate coordination, it only interacts with one oxygen atom. In bidentate bridging coordination, one metal cation interacts with one oxygen atom, and the other interacts with another. If a hydrogen atom from a water molecule replaces one of the metal cations, it becomes a pseudobridging type. Deacon and Phillips discovered an empirical rule that correlates COO^- group coordination with metal cations and the frequency separation between COO^- group's asymmetric and symmetric stretching modes ($\Delta\nu_{a-s}$).[62] Generally, it is well-known that the $\Delta\nu_{a-s}$ values of COO^- groups adsorbed on metal oxides are 200−500 cm^{-1} for monodentate, 150−180 cm^{-1} for bidentate bridging, and 60−100 cm^{-1} for bidentate chelating. The observed $\Delta\nu_{a-s}$ values in the ATR-FTIR spectra of Phg adsorbed on WO_3 nanoparticle film suggest that monodentate adsorption mode is the most probable adsorption configuration in the absence or presence of TMβCDx. On the other hand, the $\Delta\nu_{a-s}$ values of Phe adsorbed on WO_3 nanoparticle film offer monodentate binding and bidentate bridging structures of Phe molecules to the surficial W^{6+} cations in the absence and presence of TMβCDx, respectively.

Furthermore, we investigated the reversibility of the adsorption process. The adsorption process of Phg molecules on WO_3 nanoparticle film was reversible regardless of the absence or presence of TMβCDx, as the characteristic bands of Phg decreased when water was flushed after the adsorption experiment. The reversible adsorption of Phe molecules was also observed in the absence of TMβCDx. However, in the presence of TMβCDx, the characteristic bands of Phe persisted even after water flushing, and the adsorption of Phe molecules seemed to be irreversible. It is well-known that the dielectric constant of water near metal oxide surfaces is much lower than that of bulk water.[63] This decrease in dielectric constant has a direct impact on the hydration efficiency of the species adsorbed on the surface.[64] Although lacking sufficient evidence, it is probable that TMβCDx, which adsorbs as an inclusion complex of Phe, could be responsible for the departure of water molecules engaged in outer-sphere interactions from the WO_3 surface, facilitating a robust inner-sphere adsorption process. Detailed investigations are underway to gain a more comprehensive understanding of this phenomenon.

3.5. Surface-Enhanced Photochromic Phenomena of WO_3 Nanocolloid Particles by TMβCDx-Complexed Phe Molecules.

Using the above results of titration, adsorption, UV−vis absorption, and ATR-FTIR, let us discuss the photochromism mechanism in the Phe/TMβCDx/WO_3 ternary aqueous system. We can provide evidence to support the following facts: (i) The adsorptivity of TMβCDx molecules onto the WO_3 nanocolloid particles is very low; therefore, the effect of free TMβCDx molecules on the photochromic behavior is negligible (adsorption and UV−vis absorption); (ii) TMβCDx molecules can form stable host−guest inclusion complexes with Phe in bulk aqueous solution (titration); (iii) Phe molecules adsorb in two different ways on the WO_3 nanocolloid surface: they irreversibly inner-sphere adsorb via electrostatic interaction of cationic amine groups and bidentate bridging of carboxyl groups in the presence of TMβCDx, they reversibly outer-sphere adsorb via electrostatic interaction of cationic amine groups and monodentate fashion of carboxyl groups on the negatively charged WO_3 nanocolloid surface in the absence of TMβCDx (adsorption and ATR-FTIR); (iv) TMβCDx-complexed Phe molecules have a higher adsorptivity for the WO_3 nanocolloid particles than free Phe ones (adsorption); (v) the initial coloration rate due to the photochromism of the WO_3 colloid solution depends upon the concentration of Phe molecules adsorbed on the WO_3 particle surface, regardless of the absence or presence of TMβCDx (UV−vis absorption and adsorption).

Many researchers have investigated the coloration/discoloration phenomena of various WO_3 materials. Some theoretical models have been proposed to explain how the coloration occurs in WO_3 materials under UV irradiation, such as the color centers model,[65] the free electron absorption model,[66] and the double insertion/extraction model of ions and electrons.[67] Although the detailed photochromic mechanism of WO_3 materials is still controversial, the double charge intercalation/extraction model is widely accepted. Below are simplified reaction equations that interpret the photoinduced coloration mechanism of crystalline $WO_3{\cdot}2H_2O$

$$\begin{aligned} WO_3{\cdot}2H_2O &\xrightarrow{h\nu} WO_3{\cdot}(2 - x/2)H_2O + xH^+ + xe^- \\ &\quad + (x/4)O_2 \\ &\xrightarrow{h\nu} H_xW^{6+}_{1-x}W^{5+}_xO_3{\cdot}(2 - x/2)H_2O \\ &\quad + (x/4)O_2 \end{aligned} \tag{16}$$

Understanding this photochromic reaction would require considering the behavior of structured water in the lattice or absorbed water molecules from the solution, as mentioned by several researchers.[68,69] According to semiconductor band theory,[70] electrons in the valence band are excited into the conduction band, leaving holes in the valence band under persistent UV irradiation with more incredible energy than the band gap. The photogenerated holes in the valence band decompose neighboring water molecules into hydrogen ions and oxygen radicals by attenuating the H−O bond.[71] Bechinger et al.[72] argued that the reactive oxygen radicals combine to generate molecular oxygen, then diffuse into the aqueous media in molecular form. Recently, Miu et al.[73] demonstrated using density functional theory (DFT) calculations that hydrogen ions are intercalated into the W−O layer network's interstitial sites by linking to O or W atoms. The photogenerated electrons promote the reduction of W^{6+} ions into W^{5+} ions in crystalline $WO_3{\cdot}2H_2O$. Therefore, the photoinduced carriers (electron−hole pairs) give rise to the formation of substoichiometric tungsten oxide containing intercalated hydrogen ions and mixed-valence tungsten states (so-called hydrogen tungsten bronze compound).[74] The coloration mechanism in this substoichiometric compound is attributed to an intervalence charge transfer (IVCT) between W^{6+} and W^{5+} ion sites.[75] Given that the selective insertion of hydrogen ions from the organic component into the [WO_6] octahedral framework enhances photochromism under the excitation described above, it is no surprise that cationic Phe molecules adsorbed on the WO_3 surface act as an effective

Scheme 2. Schematic Illustrations of (a) Inclusion Complex between TMβCDx and AA in the Aqueous Media, (b) Phe and TMβCDx-Complexed Phe Molecules Adsorbed Onto WO_3 Nanocolloid Particles in the Phe/WO_3 Binary and Phe/TMβCDx/WO_3 Ternary Aqueous System, Respectively, and (c) Proposed Photochromic Coloration Mechanism for IVCT of WO_3 Nanocolloid Particles with TMβCDx-Complexed Phe Molecules Adsorbed on Their Surface Upon UV Irradiation

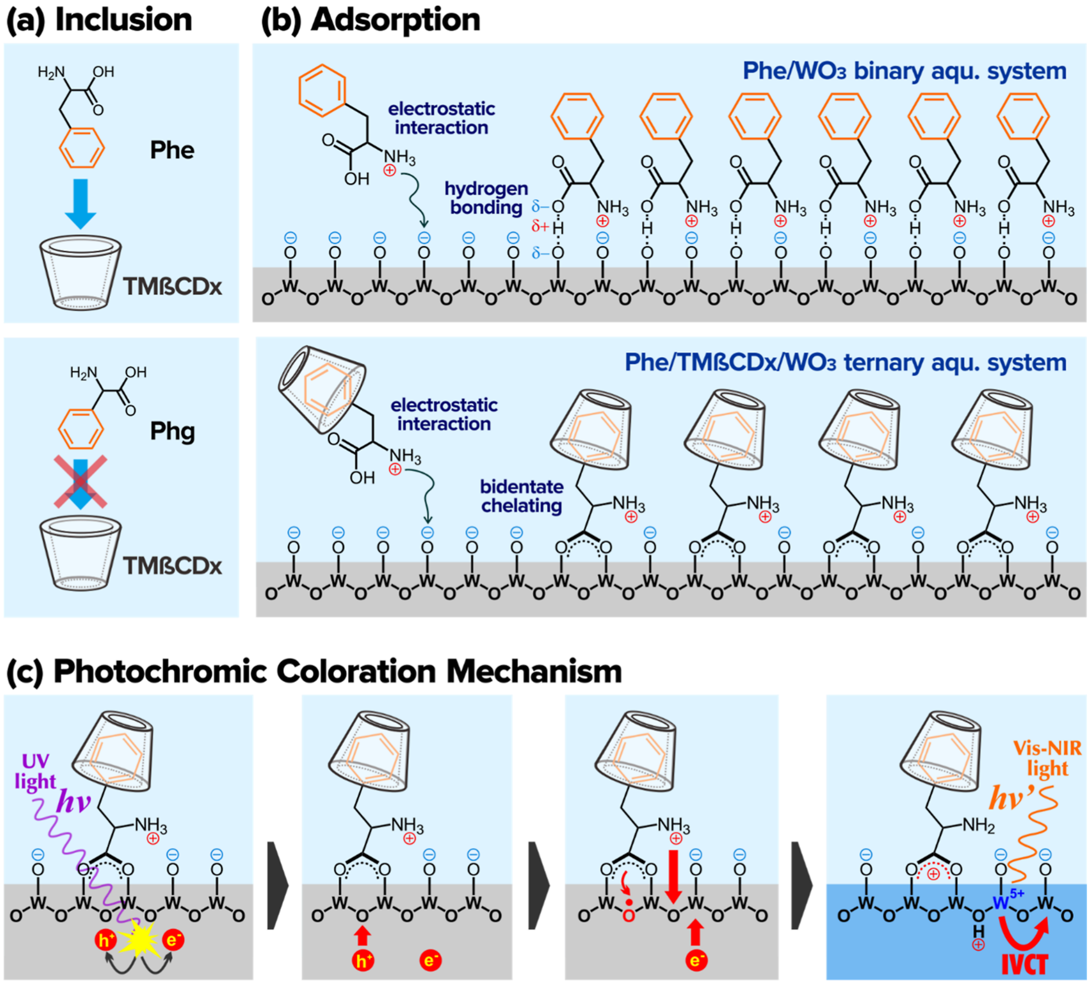

proton source and W^{6+} ions located near the $WO_3 \cdot 2H_2O$ nanocrystal surface are preferentially photoreduced.

Based on several literatures on WO_3 photochromism[76−78] and the results obtained in this study, we propose the relationship between the adsorption behavior of Phe molecules on the WO_3 surface and the photochromic behavior of WO_3 nanocolloid particles in the acidic Phe/TMβCDx/WO_3 ternary aqueous system, as shown in Scheme 2. In the bulk aqueous solution, cationic Phe molecules form inclusion complexes with TMβCDxs with 1:1 stoichiometric ratio. Competitive outer-sphere adsorption initially occurs between free cationic Phe and TMβCDx-complexed cationic Phe molecules on the negatively charged WO_3 particle surface, driven by electrostatic interactions. Stumm et al. indicated that a drastic enhancement of hydrophobicity by species adsorbed densely on the metal oxide surface promotes the release of ions (H^+/OH^-) from the surface into the adjacent bulk aqueous solution, leading to the formation of the inner-sphere complexes from the outer-sphere ones on the surface.[79] In the Phe/TMβCDx/WO_3 ternary system, dominant adsorption of hydrophobic TMβCDx-complexed cationic Phe molecules is eventually regulated by site-specific bindings consistent with bidentate bridging arrangements of carboxyl groups on the WO_3 surface via the inner-sphere adsorption mechanism, resulting in high adsorptivity of Phe molecules in the Phe/TMβCDx/WO_3 ternary aqueous system. The protonated amino group of the adsorbed Phe molecules acts as an effective proton source, which significantly enhances the coloration behavior of WO_3 nanocolloid particles by UV irradiation. Potentially, the bidentate bridging site by the carboxylate group may act more effectively as a hole trap and facilitate IVCT, as noted by Atitar et al.[58] Therefore, a highly sensitive label-free colorimetric sensing of Phe molecules has been successfully achieved using surface-enhanced photochromic phenomena, which remain unaffected by external factors such as ionic strength.

However, the complicated mechanisms governing photochromism in WO_3 materials are not fully understood, and we cannot also completely rule out the possibility of inner-sphere adsorption by bidentate bridging in the Phe/WO_3 binary aqueous system (without TMβCDx). Therefore, the proposed mechanism of surface-enhanced photochromic phenomena in the Phe/TMβCDx/WO_3 ternary aqueous system may not be sufficient. We aim to further elucidate the details of surface-enhanced photochromic phenomena by conducting more studies on adsorption and photochromism using other amino acids, similar compounds, and various inclusion compounds.

https://doi.org/10.1021/acsomega.3c09239
ACS Omega 2024, 9, 18957−18972

4. CONCLUSIONS

We have demonstrated the novel colorimetric assay system using the surface-enhanced photochromic phenomenon of WO_3 nanocolloid particles for "label-free" quantification of aromatic amino acids (AAs), L-phenylalanine (Phe) and L-2-phenylglycine (Phg), in an aqueous solution. The findings in this study provided insightful information on the causal relationship between AA-TMβCDx-WO_3 ternary interactions and surface-enhanced photochromic phenomena by amino acid molecules absorbed on the WO_3 surface. The identical linear relationship between the concentration of AAs adsorbed on the WO_3 nanocolloid particles and the initial coloration rate in the corresponding UV-irradiated colloidal WO_3 in aqueous media was observed, regardless of the presence of TMβCDx, clearly indicating that specific molecular adsorption behaviors can be converted into visually quantifiable detection signals. Notably, the highest sensitivity was found in the Phe/TMβCDx/WO_3 ternary system, with the lowest LOQ and LOD values. The detailed adsorption isotherm analysis revealed that the TMβCDx-complexed Phe molecules have significantly higher adsorptivity to the WO_3 nanocolloid particles than free Phe ones, resulting in "surface enrichment" by these molecules. Furthermore, in the Phe/TMβCDx/WO_3 ternary aqueous system, the present study identifies inner-sphere adsorption of Phe molecules via bidentate bridging bindings of carboxyl groups on the WO_3 surface strongly evidenced by both the ionic strength tests and ATR-FTIR spectroscopy. Therefore, the combination of the promoted adsorptivity and the strong inner-sphere adsorption of the TMβCDx-complexed Phe molecules successfully achieves a highly sensitive and robust colorimetric assay based on the surface-enhanced photochromic phenomenon of WO_3 nanocolloid particles. Moreover, this colorimetric platform would even be customized to detect a broad range of target molecules as well as amino acid compounds, because it can integrate with various host−guest molecule bindings. We believe that the proposed coloration mechanism of a surface-enhanced photochromic phenomenon has high potential utility and versatility in the "label-free" colorimetric analysis system, and also envisage new applications in environmental monitoring, point-of-care testing, public health screening, pharmaceutical, and biomedical fields. Further related work is in progress.

■ ASSOCIATED CONTENT

Supporting Information

The Supporting Information is available free of charge at https://pubs.acs.org/doi/10.1021/acsomega.3c09239.

Experimental details (TMβCDx-complexed aromatic amino acids, adsorption of TMβCDx on the WO_3 nanocolloid surface); UV−vis absorption spectra, Benesi−Hildebrand plots, HPLC chromatograms, XRD pattern, TEM images, surface zeta potential, and ATR-FTIR spectrum; and equilibria in the AA/TMβCDx/WO_3 ternary aqueous system (PDF)

■ AUTHOR INFORMATION

Corresponding Author

Kenta Adachi − *Department of Chemistry, Graduate School of Sciences & Technology for Innovation, Yamaguchi University, Yamaguchi 753-8512, Japan;* orcid.org/0000-0003-0298-1431; Phone: +81-83-933-5731; Email: k-adachi@yamaguchi-u.ac.jp

Authors

Hiro Azakami − *Department of Chemistry, Graduate School of Sciences & Technology for Innovation, Yamaguchi University, Yamaguchi 753-8512, Japan*

Miyuki Yamauchi − *Department of Chemistry, Graduate School of Sciences & Technology for Innovation, Yamaguchi University, Yamaguchi 753-8512, Japan*

Moeka Koshoji − *Department of Chemistry, Faculty of Science, Yamaguchi University, Yamaguchi 753-8512, Japan*

Asami Yamamoto − *Department of Environmental Science & Engineering, Graduate School of Science & Engineering, Yamaguchi University, Yamaguchi 753-8512, Japan*

Shohei Tanaka − *Department of Chemistry, Graduate School of Sciences & Technology for Innovation, Yamaguchi University, Yamaguchi 753-8512, Japan;* orcid.org/0000-0001-5112-4247

Complete contact information is available at: https://pubs.acs.org/10.1021/acsomega.3c09239

Author Contributions

K.A. designed the study, the main conceptual ideas, and the proof outline. H.A., M.Y., M.K., A.Y., and S.T. contributed to the sample preparation, measurements, data analysis, and discussion. K.A. wrote the main manuscript with inputs and helps from S.T. All authors discussed the results and commented on the manuscript.

Notes

The authors declare no competing financial interest.

■ ACKNOWLEDGMENTS

This study was financially supported in part by the Grant-in-Aid for Scientific Research (C) (grant nos. 19K05525 and 22K05154) from Japan Society for the Promotion of Science (JSPS), the Adaptable and Seamless Technology transfer Program through Target-driven R&D (A-STEP) (grant no. JPMJTM20GC) from Japan Science and Technology (JST). The authors thank the Core Clusters for Research Initiatives of Yamaguchi University, "Novel Analytical and Measuring Technology Contributions to Elucidation of Materials aiming at Life-Science Applications." TEM and XRD measurements documented in this report were performed at the Innovation Center and the Center for Instrumental Analysis, Yamaguchi University, respectively.

■ REFERENCES

(1) *Principles of Biochemistry*, 5th ed.; Moran, L. A.; Moran, L.; Horton, R.; Horton, R. A.; Rawn, D.; Scrimgeour, G.; Perry, M., Eds.; Prentice Hall, 2011.

(2) Ling, Z.-N.; Jiang, Y.-F.; Ru, J.-N.; Lu, J.-H.; Ding, B.; Wu, J. Amino acid metabolism in health and disease. *Signal Transduct. Target. Ther.* **2023**, *8*, 345.

(3) Williamson, D. *Phenylalanine: Dietary Sources, Functions and Health Effects*; Nova Science, 2015.

(4) Pode-Shakked, B.; Shemer-Meiri, L.; Harmelin, A.; Stettner, N.; Brenner, O.; Abraham, S.; Schwartz, G.; Anikster, Y. Man made disease: Clinical manifestations of low phenylalanine levels in an inadequately treated phenylketonuria patient and mouse study. *Mol. Genet. Metab.* **2013**, *110*, S66−S70.

(5) van Spronsen, F. J.; Blau, N.; Harding, C.; Burlina, A.; Longo, N.; Bosch, A. M. Phenylketonuria. *Nat. Rev. Dis. Primers* **2021**, *7*, 36.

(6) Saha, M.; Das, S. Electrochemical detection of L-serine and L-phenylalanine at bamboo charcoal−carbon nanosphere electrode. *J. Nanostruct. Chem.* **2014**, *4*, 102.

https://doi.org/10.1021/acsomega.3c09239
ACS Omega 2024, 9, 18957−18972

(7) Kamruzzaman, M.; Alam, A.-M.; Kim, K. M.; Lee, S. H.; Kim, Y. H.; Kim, G.-M.; Dang, T. D. Microfluidic chip based chemiluminescence detection of L-phenylalanine in pharmaceutical and soft drinks. *Food Chem.* **2012**, *135*, 57−62.
(8) Hasanzadeh, M.; Zargami, A.; Baghban, H. N.; Mokhtarzadeh, A.; Shadjou, N.; Mahboob, S. Aptamer-based assay for monitoring genetic disorder phenylketonuria (PKU). *Int. J. Biol. Macromol.* **2018**, *116*, 735−743.
(9) Hu, Y. F.; Zhang, Z. H.; Zhang, H. B.; Luo, L. J.; Yao, S. Z. Electrochemical determination of l-phenylalanine at polyaniline modified carbon electrode based on β-cyclodextrin incorporated carbon nanotube composite material and imprinted sol−gel film. *Talanta* **2011**, *84*, 305−313.
(10) Yıldırım, M.; Bölükbaşı, Ö. S.; Parlak Özer, Z.; Polat, I.·.; Atar, N.; Yola, M. L. l-Phenylalanine-Imprinted Electrochemical Sensor Based on WS_2 Nanoflowers on N,B-Doped Graphene and Its Application to Milk Samples. *Ind. Eng. Chem. Res.* **2023**, *62* (11), 4587−4594.
(11) Messina, M. A.; Meli, C.; Conoci, S.; Petralia, S. A Facile Method for Urinary Phenylalanine Measurement on Paper-Based Lab-on-Chip for PKU Therapy Monitoring. *Analyst* **2017**, *142* (24), 4629−4632.
(12) Kand'ár, R.; Žáková, P. Determination of Phenylalanine and Tyrosine in Plasma and Dried Blood Samples Using HPLC with Fluorescence Detection. *J. Chromatogr. B: Anal. Technol. Biomed. Life Sci.* **2009**, *877*, 3926−3929.
(13) Zhang, K.; Yan, H.-T.; Zhou, T. Spectrofluorimetric Determination of Phenylalanine Based on Fluorescence Enhancement of Europium Ion Immobilized With Sol−Gel Method. *Spectrochim. Acta, Part A* **2011**, *83*, 155−160.
(14) Arakawa, T.; Koshida, T.; Gessei, T.; Miyajima, K.; Takahashi, D.; Kudo, H.; Yano, K.; Mitsubayashi, K. Biosensor for L-Phenylalanine Based on the Optical Detection of NADH Using a UV Light Emitting Diode. *Microchim. Acta* **2011**, *173*, 199−205.
(15) Çimen, D.; Bereli, N.; Denizli, A. Surface Plasmon Resonance Based on Molecularly Imprinted Polymeric Film for L-Phenylalanine Detection. *Biosensors* **2021**, *11*, 21.
(16) Hsu, L.-W.; Lin, Y.-H.; Guo, J.-Y.; Chen, C.-F.; Chou, Y.-J.; Yeh, Y.-C. Simultaneous Determination of l-Phenylalanine, Phenylethylamine, and Phenylacetic Acid Using Three-Color Whole-Cell Biosensors within a Microchannel Device. *ACS Appl. Bio Mater.* **2020**, *3*, 5120−5125.
(17) Yang, J.; Wang, K.; Xu, H.; Yan, W.; Jin, Q.; Cui, D. Detection platforms for point-of-care testing based on colorimetric, luminescent and magnetic assays: A review. *Talanta* **2019**, *202*, 96−110.
(18) Syedmoradi, L.; Daneshpour, M.; Alvandipour, M.; Gomez, F. A.; Hajghassem, H.; Omidfar, K. Point of care testing: The impact of nanotechnology. *Biosens. Bioelectron.* **2017**, *87*, 373−387.
(19) Haleem, A.; Javaid, M.; Singh, R. P.; Rab, S.; Suman, R. Applications of nanotechnology in medical field: a brief review. *Glob. Health J.* **2023**, *7*, 70−77.
(20) Kayani, A. B. A.; Kuriakose, S.; Monshipouri, M.; Khalid, F. A.; Walia, S.; Sriram, S.; Bhaskaran, M. UV Photochromism in Transition Metal Oxides and Hybrid Materials. *Small* **2021**, *17*, 2100621.
(21) He, T.; Yao, J. Photochromism in composite and hybrid materials based on transition-metal oxides and polyoxometalates. *Prog. Mater. Sci.* **2006**, *51*, 810−879.
(22) Zappa, D.; Galstyan, V.; Kaur, N.; Munasinghe Arachchige, H. M. M.; Sisman, O.; Comini, E. Metal Oxide -Based Heterostructures for Gas Sensors"- A Review. *Anal. Chim. Acta* **2018**, *1039*, 1−23.
(23) Wang, Y.; Runnerstrom, E. L.; Milliron, D. J. Switchable Materials for Smart Windows. *Annu. Rev. Chem. Biomol. Eng.* **2016**, *7*, 283−304.
(24) Wang, S.; Fan, W.; Liu, Z.; Yu, A.; Jiang, X. Advances on tungsten oxide based photochromic materials: strategies to improve their photochromic properties. *J. Mater. Chem. C* **2018**, *6*, 191−212.
(25) Pacheco, M. L.; Pinto, T. V.; Sousa, C. M.; Guedes, A.; Blanco, G.; Pintado, J. M.; Coelho, P. J.; Freire, C.; Pereira, C. R. Tuning the Photochromic Properties of WO3-Based Materials toward High-Performance Light-Responsive Textiles. *ACS Appl. Opt. Mater.* **2023**, *1* (8), 1434−1451.
(26) Cui, B.; Guo, C.; Fu, G.; Zhang, Z. Photochromic performance of hydrogel based on deep eutectic solvent induced water soluble Cu-doped WO_3 hybrids with antibacterial property. *J. Photochem. Photobiol., A* **2023**, *435*, 114320.
(27) Adachi, K.; Tokushige, M.; Omata, K.; Yamazaki, S.; Iwadate, Y. Kinetics of Coloration in Photochromic Tungsten(VI) Oxide/Silicon Oxycarbide/Silica Hybrid Xerogel: Insight into Cation Self-diffusion Mechanisms. *ACS Appl. Mater. Interfaces* **2016**, *8*, 14019−14028.
(28) Yamamoto, A.; Adachi, K. Label-free Colorimetric Sensing of α-Amino Acids Based on Surface-enhanced Photochromic Phenomena of Molybdenum(VI) Oxide Nanoparticles. *Bunseki Kagaku* **2017**, *66*, 639−646.
(29) Tanaka, S.; Adachi, K.; Yamazaki, S. Surface-enhanced photochromic phenomena of phenylalanine adsorbed on tungsten oxidenanoparticles: a novel approach for "label-free" colorimetric sensing. *Analyst* **2013**, *138*, 2536−2539.
(30) *Cyclodextrins and Their Complexes: Chemistry, Analytical Methods, Applications*; Dodziuk, H., Ed.; John Wiley & Sons, 2006.
(31) Crini, G. Review: A History of Cyclodextrins. *Chem. Rev.* **2014**, *114*, 10940−10975.
(32) Marques, H. M. C. A review on cyclodextrin encapsulation of essential oils and volatiles. *Flavour Fragr. J.* **2010**, *25*, 313−326.
(33) Morimoto, M.; Bierschenk, S. M.; Xia, K. T.; Bergman, R. G.; Raymond, K. N.; Toste, F. D. Advances in Supramolecular Host-mediated Reactivity. *Nat. Catal.* **2020**, *3*, 969−984.
(34) Zhou, J.; Tang, J.; Tang, W. Recent Development of Cationic Cyclodextrins for Chiral Separation. *TrAC, Trends Anal. Chem.* **2015**, *65*, 22−29.
(35) Bjerre, J.; Rousseau, C.; Marinescu, L.; Bols, M. Artificial enzymes, "Chemzymes": current state and perspectives. *Appl. Microbiol. Biotechnol.* **2008**, *81*, 1−11.
(36) Adachi, K.; Watarai, H. Site-Selective Formation of Optically Active Inclusion Complexes of Alkoxo-Subphthalocyanines with β-Cyclodextrin at the Toluene/Water Interface. *Chem. Eur. J.* **2006**, *12*, 4249−4260.
(37) Adachi, K.; Mita, T.; Yamate, T.; Yamazaki, S.; Takechi, H.; Watarai, H. Controllable Adsorption and Ideal H-Aggregation Behaviors of Phenothiazine Dyes on the Tungsten Oxide Nanocolloid Surface. *Langmuir* **2010**, *26*, 117−125.
(38) Adachi, K.; Tanaka, S.; Yamazaki, S.; Takechi, H.; Tsukahara, S.; Watarai, H. Chirality Induction and Amplification in Methylene Blue H-Aggregates via D- and L-Phenylalanine Pre-Adsorbed on the Tungsten Oxide Nanocolloid Surface. *New J. Chem.* **2012**, *36*, 2167−2170.
(39) Wolcott, A.; Kuykendall, T. R.; Chen, W.; Chen, S.; Zhang, J. Z. Synthesis and Characterization of Ultrathin WO_3 Nanodisks Utilizing Long-Chain Poly(ethylene glycol). *J. Phys. Chem. B* **2006**, *110*, 25288−25296.
(40) Kosmulski, M. *Chemical Properties of Material Surfaces*; Marcel Dekker, 2001.
(41) McQuillan, A. J.; Osawa, M.; Peak, D.; Ren, B.; Tian, Z.-Q. Experiments on adsorption at hydrous metal oxide surfaces using attenuated total reflection infrared spectroscopy (ATRIRS) (IUPAC Technical Report). *Pure Appl. Chem.* **2019**, *91*, 2043−2061.
(42) Platt, J. R. Classification of Spectra of Cata-Condensed Hydrocarbons. *J. Chem. Phys.* **1949**, *17*, 484−495.
(43) Süß, F.; Kahle, C.; Holzgrabe, U.; Scriba, G. K. E. Studies on the chiral recognition of peptide enantiomers by neutral and sulfated β-cyclodextrin and heptakis-(2,3-di-O-acetyl)-β-cyclodextrin using capillary electrophoresis and nuclear magnetic resonance. *Electrophoresis* **2002**, *23*, 1301−1307.
(44) Kahle, C.; Holzgrabe, U. Determination of binding constants of cyclodextrin inclusion complexes with amino acids and dipeptides by potentiometric titration. *Chirality* **2004**, *16*, 509−515.
(45) Rekharsky, M. V.; Inoue, Y. Complexation Thermodynamics of Cyclodextrins. *Chem. Rev.* **1998**, *98*, 1875−1918.

(46) Song, L. X.; Teng, C. F.; Yang, Y. Preparation and Characterization of the Solid Inclusion Compounds of α-β-Cyclodextrin with Phenylalanine (D-L- and DL-Phe) and Tryptophan (D-L- and DL-Trp). *J. Incl. Phenom. Macrocycl. Chem.* **2006**, *54*, 221−232.
(47) Parks, G. A. The Isoelectric Points of Solid Oxides, Solid Hydroxides, and Aqueous Hydroxo Complex Systems. *Chem. Rev.* **1965**, *65*, 177−198.
(48) Georg, A.; Graf, W.; Wittwer, V. Comparison of electrical conductivity and optical properties of substoichiometrically and electrochemically coloured WO_x films of different crystallinity. *Sol. Energy Mater. Sol. Cells* **1998**, *51*, 353−370.
(49) ISO 11843 Part 7 Methodology based on stochastic properties of instrumental noise.
(50) Huang, C. P.; O'Melia, C. R.; Morgan, J. J. *Aquatic Chemistry: Interfacial and Interspecies Processes*; American Chemical Society, 1995.
(51) Goldberg, S. Application of surface complexation models to anion adsorption by natural materials. *Environ. Toxicol. Chem.* **2014**, *33*, 2172−2180.
(52) Tolstoy, V. P.; Chernyshova, I.; Skryshevsky, V. A. *Handbook of Infrared Spectroscopy of Ultrathin Films*; Wiley-Interscience, 2003.
(53) Socrates, G. *Infrared and Raman Characteristic Group Frequencies: Tables and Charts*; 3rd ed.; John Wiley & Sons, 2001.
(54) Silverstein, R. M.; Bassler, G. C.; Morrill, T. C. *Spectrometric Identification of Organic Compounds*; 5th ed.; John Wiley & Sons, 1991.
(55) Olsztyńska-Janus, S.; Komorowska, M. Conformational changes of L-phenylalanine induced by near infrared radiation. ATR-FTIR studies. *Struct. Chem.* **2012**, *23*, 1399−1407.
(56) Barth, A. The infrared absorption of amino acid side chains. *Prog. Biophys. Mol. Biol.* **2000**, *74*, 141−173.
(57) *CRC Handbook of Chemistry and Physics* 91st ed.; Haynes, W. M., Ed.; CRC Press, 2010.
(58) Atitar, M. F.; Dillert, R.; Bahnemann, D. W. Surface Interactions between Imazapyr and the TiO_2 Surface: An in Situ ATR-FTIR Study. *J. Phys. Chem. C* **2017**, *121*, 4293−4303.
(59) Rajalakshmi, S.; Pitchaimuthu, S.; Kannan, N.; Velusamy, P. Enhanced photocatalytic activity of metal oxides/β-cyclodextrin nanocomposites for decoloration of Rhodamine B dye under solar light irradiation. *Appl. Water Sci.* **2017**, *7*, 115−127.
(60) Nakamoto, K. *Infrared and Raman Spectra of Inorganic and Coordination Compounds: Part A: Theory and Applications in Inorganic Chemistry*; John Wiley & Sons, 2009.
(61) Tackett, J. E. FT-IR Characterization of Metal Acetates in Aqueous Solution. *Appl. Spectrosc.* **1989**, *43*, 483−489.
(62) Deacon, G. B.; Phillips, R. J. Relationships between the carbon-oxygen stretching frequencies of carboxylato complexes and the type of carboxylate coordination. *Coord. Chem. Rev.* **1980**, *33*, 227−250.
(63) Teschke, O.; Ceotto, G.; de Souza, E. F. Interfacial water dielectric-permittivity-profile measurements using atomic force microscopy. *Phys. Rev. E* **2001**, *64*, 011605.
(64) Angelova, S.; Nikolova, V.; Pereva, S.; Spassov, T.; Dudev, T. α-Cyclodextrin: How Effectively Can Its Hydrophobic Cavity Be Hydrated? *J. Phys. Chem. B* **2017**, *121* (39), 9260−9267.
(65) Deb, S. K. Optical and photoelectric properties and colour centres in thin films of tungsten oxide. *Philos. Mag.* **1973**, *27*, 801−822.
(66) Svensson, J. S. E. M.; Granqvist, C. G. Electrochromic Coatings for Smart Windows: Crystalline and Amorphous WO_3 Films. *Thin Solid Films* **1985**, *126*, 31−36.
(67) Bange, K. Colouration of tungsten oxide films: A model for optically active coatings. *Sol. Energy Mater. Sol. Cells* **1999**, *58*, 1−131.
(68) Gavrilyuk, A. Aging of the nanosized photochromic WO3 films and the role of adsorbed water in the photochromism. *Appl. Surf. Sci.* **2016**, *364*, 498−504.
(69) Bechinger, C.; Oefinger, G.; Herminghaus, S.; Leiderer, P. On the fundamental role of oxygen for the photochromic effect of WO_3. *J. Appl. Phys.* **1993**, *74*, 4527−4533.
(70) Zych, M.; Syrek, K.; Pisarek, M.; Sulka, G. D. Synthesis and Characterization of Anodic WO3 Layers in Situ Doped with C, N during Anodization. *Electrochim. Acta* **2022**, *411*, 140061.
(71) Katsumata, H.; Tachi, Y.; Suzuki, T.; Kaneco, S. Z-scheme Photocatalytic Hydrogen Production over WO_3/g-C_3N_4 Composite Photocatalysts. *RSC Adv.* **2014**, *4*, 21405−21409.
(72) Bechinger, C.; Oefinger, G.; Herminghaus, S.; Leiderer, P. On the Fundamental Role of Oxygen for the Photochromic Effect of WO_3. *J. Appl. Phys.* **1993**, *74*, 4527−4533.
(73) Miu, E. V.; McKone, J. R.; Mpourmpakis, G. The Sensitivity of Metal Oxide Electrocatalysis to Bulk Hydrogen Intercalation: Hydrogen Evolution on Tungsten Oxide. *J. Am. Chem. Soc.* **2022**, *144* (14), 6420−6433.
(74) Xi, Y.; Zhang, Q.; Cheng, H. Mechanism of Hydrogen Spillover on WO_3(001) and Formation of H_xWO_3 (x = 0.125, 0.25, 0.375, and 0.5). *J. Phys. Chem. C* **2014**, *118*, 494−501.
(75) Brunschwig, B. S.; Sutin, N. Energy surfaces, reorganization energies, and coupling elements in electron transfer. *Coord. Chem. Rev.* **1999**, *187*, 233−254.
(76) Adachi, K.; Mita, T.; Tanaka, S.; Honda, K.; Yamazaki, S.; Nakayama, M.; Goto, T.; Watarai, H. Kinetic characteristics of enhanced photochromism in tungsten oxide nanocolloid adsorbed on cellulose substrates, studied by total internal reflection Raman spectroscopy. *RSC Adv.* **2012**, *2*, 2128−2136.
(77) Ling, Z.; Liu, K.; Zou, Q.; Li, Q.; Zhang, K.-Q.; Cui, Z.; Yuan, W.; Liu, Y. Continuous and rapid fabrication of photochromic fibers by facilely coating tungsten oxide/polyvinyl alcohol composites. *RSC Adv.* **2018**, *8*, 28581−28587.
(78) Yamazaki, S.; Isoyama, K. Kinetic Studies of WO_3-Based Photochromism in Polyvinyl Alcohol Film. *Langmuir* **2023**, *39*, 10240−10248.
(79) Stumm, W.; Kummert, R.; Sigg, L. A Ligand-Exchange Model for the Adsorption of Inorganic and Organic-Ligands at Hydrous Oxide Interfaces. *Croat. Chem. Acta* **1980**, *53*, 291−312.

https://doi.org/10.1021/acsomega.3c09239
ACS Omega 2024, 9, 18957−18972